J. Fluid Mech. (1988), *vol.* 197, *pp.* 259–293
Printed in Great Britain

The effect of small surface perturbations on the pulsatile boundary layer on a semi-infinite flat plate

By P. W. DUCK
Department of Mathematics, University of Manchester, Manchester M13 9PL, UK

(Received 6 March 1986 and in revised form 11 March 1988)

The laminar pulsatile flow over a semi-infinite flat plate, on which is located a small (steady) surface distortion is investigated; triple-deck theory provides the basis for the study. The problem is of direct relevance to the externally imposed acoustic excitation of boundary layers. The investigation is primarily numerical and involves the solution of the nonlinear, unsteady boundary-layer equations which arise from the lower deck. The numerical method involves the use of finite differencing in the transverse direction, Crank–Nicolson marching in time, and Fourier transforms in the streamwise direction, and as such is an extension of the spectral method of Burggraf & Duck (1982). Supersonic and incompressible flows are studied. A number of the computations presented suggest that the small surface distortion can excite a large-wavenumber, rapidly growing instability, leading to a breakdown of the solution, with the wall shear at a point seeming to increase without bound as a finite time is approached. Rayleigh modes for the basic (undisturbed) velocity profile are computed and there is some correlation between the existence and magnitude of the growth rate of these unstable modes, and the occurrence of the apparent singularity. Streamline plots indicate that this phenomenon is linked to the formation of closed (or 'cats-eye') eddies in the main body of the boundary layer, away from the wall. Tollmien–Schlichting instabilities are clearly seen in the case of incompressible flows.

1. Introduction

The problem investigated is that of pulsatile flow past a semi-infinite flat plate on which is situated a small distortion, distance L from the leading edge. The free-stream velocity is taken to be $U_\infty(1+\lambda \sin \Omega t^*, 0)$, (with U_∞ constant), referred to Cartesian coordinates $(x^*, y^*) = L(x+1, y)$, origin at the leading edge, with the undistorted plate lying along $y^* = 0$. The general velocity vector is then taken as $U_\infty(u, v)$, where it is assumed there is no velocity (or solution variation) in the cross-flow (z^*) direction. The kinematic viscosity of the fluid in the free stream is ν_0, and non-dimensional time $t = \Omega t^*$. The problem, as stated, involves three non-dimensional parameters, namely a frequency parameter

$$\beta_0 = \left(\frac{U_\infty}{\Omega L}\right)^{\frac{1}{2}} \tag{1.1}$$

($\beta_0 \to 0$ representing increasingly faster oscillations, $\beta_0 \to \infty$ representing increasingly slower oscillations), a Reynolds number

$$R = \frac{U_\infty L}{\nu_0}, \tag{1.2}$$

which is assumed large throughout this paper, and finally the oscillation amplitude parameter λ. When considering the so-called triple-deck problem, it is convenient to introduce a small parameter ϵ, related to the Reynolds number by

$$\epsilon = R^{-\frac{1}{8}}. \tag{1.3}$$

The basic flow (i.e. the flow without the inclusion of the distortion) itself is of much interest, most of the work on this being for the incompressible case with $\lambda \ll 1$ (i.e. a small oscillatory component). The various phases of the flow (for the incompressible case) are clearly identified by Goldstein (1983) (see in particular his figure 1). The first is of streamwise dimension $O(U_\infty \bar{\epsilon}/\Omega)$, centred around the leading edge (where $\bar{\epsilon} = (\nu_0 \Omega/U_\infty^2)^{\frac{1}{2}}$), and is a region in which the full Navier–Stokes equations apply. The second region, at a distance $O(U_\infty/\Omega)$ from the leading edge is perhaps the most studied region, with the flow governed by the unsteady boundary-layer equations. This has been investigated by Lighthill (1954), Lam & Rott (1960) and Ackerberg & Phillips (1972). Downstream the solution develops a double structure: to leading order the inner layer is a Stokes' layer, whilst the outer layer is a Blasius motion. Ackerberg & Phillips (1972) and Goldstein, Pockol & Sanz (1983) have obtained numerical solutions for the linearized case $\lambda \ll 1$, from the leading edge to far downstream. (The problem for compressible flow past a hot flat plate at zero incidence has been treated by Illingworth 1958.)

Lam & Rott (1960) noted that the downstream inner (Strokes) solution must be 'incomplete', since it is determined without recourse to upstream conditions, and hence a set of eigensolutions which decay exponentially fast in the streamwise direction must be present. One set of eigensolutions was found by Lam & Rott (1960) and Ackerberg & Phillips (1972), whose eigenfunctions were dominated by conditions at the wall, and whose decay rate decreases as the eigenvalue increases. Brown & Stewartson (1973*a*, *b*) found an alternative set of asymptotic eigensolutions, whose eigenfunctions were dominated by conditions at the outer reaches of the boundary layer, and whose exponential decay rate increases with increasing order. It does not appear that these two alternative descriptions of the flow have been fully reconciled as yet.

The eigensolutions of Lam & Rott (1960) and Ackerberg & Phillips (1972) are proportional to $\exp(-\lambda_0(\Omega x^*/U_\infty)^{\frac{1}{2}})$, where λ_0 is a complex constant, and so oscillate with a wavelength proportional to $x^{*-\frac{1}{2}}$. At the same time the outer (Blasius) boundary-layer thickness must grow as $x^{*\frac{1}{2}}$. Thus the streamwise scale of the unsteady component of the motion must ultimately become comparable with the boundary-layer thickness; as a result cross-stream pressure fluctuations, neglected in the boundary layer approximation must become important for sufficiently large x^*. These eigensolutions will then no longer be a valid approximation to the Navier–Stokes equations. This aspect was considered by Goldstein (1983), who showed that for $x^* = O[U_\infty \bar{\epsilon}^{-2}/\Omega]$, (i.e. much further downstream than the unsteady boundary-layer zone), the (perturbation) flow becomes governed by the Orr–Sommerfeld equation, involving Tollmien–Schlichting waves which initially decay, but then ultimately grow for sufficiently large x^*. Goldstein (1983) showed that an overlap region exists between the boundary-layer region and the Orr–Sommerfeld region, and illustrated how long-wavelength free-stream disturbances can trigger Tollmien–Schlichting waves of much shorter wavelength (related aspects of this problem have been considered by Murdock 1980 and Goldstein *et al.* 1983).

The case of $\lambda = O(1)$ has also received attention in the asymptotic limits equivalent to close to the leading edge (Moore 1951, 1957; Pedley 1972) and far from

the leading edge (Lin 1956; Gibson 1957; Pedley 1972). This particular problem is considered at all distances from the leading edge by the author in a forthcoming paper.

A number of papers presenting triple-deck studies involving the effect of unsteadiness have been presented. For example Brown & Daniels (1975) and Brown & Cheng (1981) have considered the effects of unsteadiness on a trailing-edge flow. Duck (1978, 1981) investigated the effect of a small oscillating disturbance on an otherwise steady (incompressible) flow, the solution being obtained asymptotically in the limit of increasingly fast oscillations. A number of Russian authors (Zhuk & Ryzhov 1978; Terent'ev 1978, 1984; Ryzhov & Zhuk 1980; Bogdanova & Ryzhov 1983), have considered a number of problems of this class, for the limit of diminishingly small distortion height (compared with the lower-deck thickness). In all these studies, purely time-periodic solutions were sought. More recently in Duck (1985*a*, hereinafter referred to as I), and Duck (1986) numerical studies of the incompressible and supersonic nonlinear flow over a small unsteady hump have been carried out (with scalings again based on triple-deck theory). In the supersonic case it was found that above some critical height of distortion, a short-wavelength instability may be triggered (this being a nonlinear effect). The work of Smith & Bodonyi (1985) and Tutty & Cowley (1986) suggests that this effect is an inviscid, Rayleigh, short-wavelength instability phenomenon. For the incompressible case it was shown in I (and by Terent'ev 1985) that Tollmien–Schlichting waves were triggered by the motion (even in the linearized case of diminishingly small distortion height), and Duck (1986) suggested that these waves could themselves be subject to a secondary (large-wavenumber) instability through nonlinearity. As a result incompressible calculations of this class tend to be a good deal more difficult than their supersonic counterparts. Indeed, it has been shown by Smith (1979*a*, *b*) that the large-Reynolds-number limit of the neutral stability curve of the Blasius boundary layer (lower branch) can be described by means of a triple-deck structure. More recently Smith & Burggraf (1985), Smith (1986), Stewart & Smith (1987), and Smith & Stewart (1987) have considered various aspects of the evolution of Tollmien–Schlichting waves, for increasingly high frequencies, based upon triple-deck theory. Taken together, these papers strongly suggest that triple-deck theory can provide a rational model for a description of the early stages of some boundary-layer transition processes.

In the studies cited above, the basic (i.e. undisturbed) flow was steady in all cases (typically the Blasius boundary layer). However in this paper the basic flow comprises a steady plus an oscillatory component. Although the oscillatory component is taken to be quite small in the free stream, scalings are chosen such that close to the surface of the plate the unsteady velocity component becomes comparable with the mean (steady) velocity component and unsteadiness is shown to have a profound effect on the flow when the surface of the plate is distorted. Here the distortion is taken to be steady, and the unsteady forcing is provided by the external flow. This is in contrast to I and Duck (1986) and a number of other papers cited above where the unsteadiness was applied through the distortion. (Here the distortion could perhaps be interpreted as a surface roughness on the plate.)

The frequency of the free-stream velocity component is chosen to be such that the corresponding Stokes-layer thickness is comparable with the thickness of the lower deck of the triple deck (as in I); this then provokes a resonance type of situation. Duck (1980, 1985*b*) and Cowley (1981, 1985) have considered analogous pulsatile channel flow problems, and these papers point to some possible interesting effects.

The primary motivation for tackling this problem lies in the important area of externally imposed acoustic excitation of boundary layers; such a problem, also based on a triple-deck model has been considered by Goldstein (1985). However, Goldstein's analysis was based on a double linearization process – first the amplitude of oscillation of the excitation was taken to be small, and then the distortion height was taken to be small, which then permitted progress to be made analytically. The present paper may be thought of as extending Goldstein's analysis into a nonlinear regime.

A further motivation for tackling the problem could be in modelling free-stream turbulence, with the velocity fluctuations being approximated by a cosinusoidal form; however the technique to be described could be extended to treat much more general situations, where the velocity fluctuations are prescribed by (for example) a Fourier time series.

Finally, throughout this paper reference will be made to locations 'upstream' and 'downstream'. In the context of reversing flows, these two terms are not well defined; however here the free-stream flow (which does not reverse direction) is taken as a reference.

2. Problem formulation

In this section the scales of the appropriate physical parameters are chosen in order to obtain the maximum amount of physical interaction inside the lower deck. The full details of the scalings for the triple deck are now well known, and may be found in Smith (1973), for example.

As in I, the frequency parameter is chosen to be such that the unsteady (Stokes') layer is of thickness comparable with the lower deck, i.e.

$$\beta_0 = \epsilon\beta, \tag{2.1}$$

where $\beta = O(1)$. This determines the magnitude of the lengthscale L to be $O[(U_\infty/\Omega)\, R^{\frac{1}{8}}]$, this being the distance from the leading edge of the plate to the wall distortion. This corresponds to the 'overlap region' of figure 1 of Goldstein (1983), and is the same location of the wall disturbance as was considered by Goldstein (1985). Following I again, the height and length of the wall perturbation are taken to be of the same order as the thickness and length of the lower deck respectively; specifically the distortion is given by

$$y = \epsilon^5 hF(X), \quad X = x/\epsilon^3 = (x^*-L)/\epsilon^3 L, \tag{2.2}$$

where h, $|F(X)|$ and X are taken to be $O(1)$ quantities generally . The final parameter scaling is that of the amplitude of the velocity oscillation λ, and this is chosen to be $O(\epsilon)$ by setting

$$\lambda = \epsilon\gamma, \quad \gamma = O(1) \tag{2.3}$$

(in the case of supersonic flows the definition of γ may also include an additional multiplicative constant reflecting density variations across the main deck). This ensures that the amplitude of oscillation of the fluid particles in the free stream is comparable with the length of the distortion (see also Duck 1985*b*).

With these scalings, and distortions of the class (2.2), the flow takes on the well-known triple-deck structure (see, for example Stewartson 1969 and Stewartson & Williams 1969). The general layout of the problem is sketched in figure 1. The

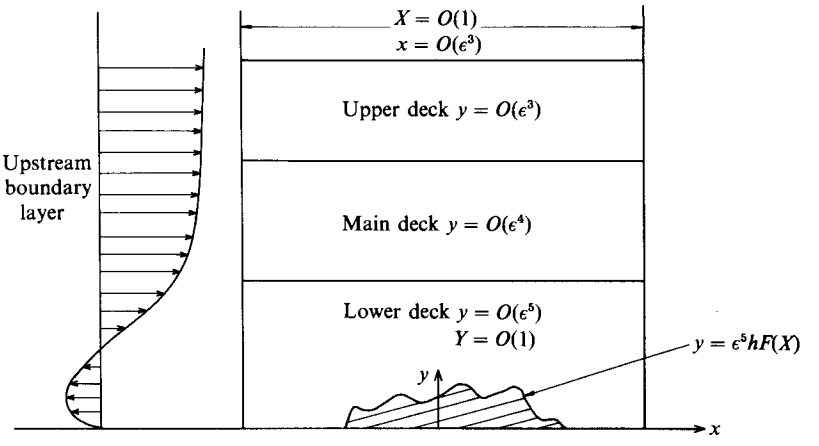

FIGURE 1. Layout of the problem.

problem reduces to the solution of the lower-deck problem wherein the velocity and pressure develop as

$$\left.\begin{aligned} u &= \epsilon U(X,Y,t)+O(\epsilon^2),\\ v &= \epsilon^3 V(X,Y,t)+O(\epsilon^4),\\ p &= \epsilon^2 P(X,t)+O(\epsilon^3). \end{aligned}\right\} \tag{2.4}$$

If the Prandtl transposition theorem is implemented, the problem reduces to

$$\frac{1}{\beta^2}U_t+UU_X+VU_Y = U_{YY}-P_X, \tag{2.5}$$

$$U_X+V_Y = 0, \tag{2.6}$$

with $$U = V = 0 \quad \text{on} \quad Y = 0,$$

$$U \to Y+A(X,t)+hF(X)+\gamma\cos t \quad \text{as} \quad Y\to\infty. \tag{2.7}$$

It is assumed that the boundary layer returns to its undisturbed state as $X\to-\infty$, and so

$$\left.\begin{aligned} &U\to U_0(Y,t),\\ &V\to 0, \quad P\to\frac{\gamma X\sin t}{\beta^2} \end{aligned}\right\} \quad \text{as} \quad X\to-\infty, \tag{2.8}$$

where $$U_0(Y,t) = Y+\{\tfrac{1}{2}\gamma[1-\mathrm{e}^{-(1+\mathrm{i})Y/\sqrt{2\beta}}]\mathrm{e}^{\mathrm{i}t}+\text{c.c.}\}, \tag{2.9}$$

where quantities have been scaled in such a way that U_{0Y} $(Y\to\infty)$ is unity.

The problem is closed by a pressure $(P(X,t))$ – displacement $(A(X,t))$ relationship, obtained by solving in the upper deck and matching with the main deck. In the case of incompressible flows this is

$$P(X,t) = \frac{1}{\pi}\int_{-\infty}^{\infty}\frac{A_\xi\,\mathrm{d}\xi}{X-\xi}\,\mathrm{d}\xi+\frac{\gamma X\sin t}{\beta^2}, \tag{2.10}$$

whilst for supersonic flows

$$P(X,t) = -A_X(X,t)+\frac{\gamma X\sin t}{\beta^2}. \tag{2.11}$$

Notice that the pressure comprises two components: a known component driving the free-stream velocity fluctuations, i.e. $(\gamma X/\beta^2)\sin t$; and an unknown component due to the presence of the wall distortion.

In general the solution of (2.5) and (2.6) must be obtained numerically (although in §4 it will be shown that some analytic progress is possible in the limit as $\beta \to 0$, providing a partial analytical check on the numerical results). In particular a numerical scheme is required that will handle reversed flow quickly and simply, since the basic flow (2.9) itself will reverse at certain times in the cycle if $\gamma/\beta > 1$. In the following section such a scheme is described.

3. Numerical method

A numerical solution of (2.5)–(2.8) is now considered. In I and Duck (1986) the Fourier transform method of Burggraf & Duck (1982) was extended to unsteady flows. In the present paper, the undisturbed flow comprises a uniform (steady) shear, together with an unsteady Stokes'-flow component; this is in contrast to these previous papers where the basic flow was a uniform shear. Further, analytic progress does not appear possible generally in the present problem, even for the linearized $(h \to 0)$ case (unlike in I), and so this too demands a fully numerical approach.

The scheme to be used is similar to that of I and Duck (1986) and so details will be kept to a minimum, whilst significant differences will be emphasized. Differentiating (2.5) with respect to Y gives

$$\frac{1}{\beta^2}\tau_t + U\tau_X + V\tau_Y = \tau_{YY}, \tag{3.1}$$

where $\tau = U_Y$ represents the shear. The flow quantities are written

$$\left.\begin{aligned} \tau &= \tau_0(Y,t) + \tilde{\tau}(X,Y,t), \\ U &= U_0(Y,t) + \tilde{U}(X,Y,t), \quad V = \tilde{V}(X,Y,t), \\ P &= \frac{\gamma X \sin t}{\beta^2} + \tilde{P}(X,t). \end{aligned}\right\} \tag{3.2}$$

Here subscript zero denotes undisturbed quantities; U_0 is defined by (2.9), and

$$\tau_0(Y,t) = 1 + \left\{\frac{\gamma(1+\mathrm{i})}{2\sqrt{2}\beta}\,\mathrm{e}^{-(1+\mathrm{i})Y/\sqrt{2}\beta + \mathrm{i}t} + \text{c.c.}\right\}. \tag{3.3}$$

Quantities with a tilde denote perturbation values; as $h \to 0$, these will be $O(h)$, but for $h = O(1)$ are themselves $O(1)$.

Substitution of (3.2) into (3.1) yields

$$\begin{aligned} \frac{1}{\beta^2}\tilde{\tau}_t + U_0\tilde{\tau}_X + \tau_{0Y}\tilde{V} - \tilde{\tau}_{YY} &= -(\tilde{U}\tilde{\tau}_X + \tilde{V}\tilde{\tau}_Y) \\ &= \tilde{R} \end{aligned} \tag{3.4}$$

(since the undisturbed flow satisfies Stokes' equation). The condition (2.7) demands

$$\tilde{U} \to A(X,t) + hF(X) \quad \text{as} \quad Y \to \infty, \tag{3.5}$$

and the relation between the pressure and the displacement function is written symbolically as

$$P = \mathscr{L}\{A\}, \tag{3.6}$$

where $\mathscr{L}\{\ \}$ denotes some linear operation. If $h \to 0$, the $O(h)$ approximation to the perturbation quantities is obtained by setting $\tilde{R} = 0$.

Taking the Fourier transform of (3.4) in the X direction yields

$$\frac{1}{\beta^2}\tilde{\tau}_t^* + \mathrm{i}kU_0\tilde{\tau}^* + \tau_{0Y}\tilde{V}^* - \tilde{\tau}_{YY}^* = -(\tilde{U}\tilde{\tau}_X + \tilde{V}\tilde{\tau}_Y)^* = \tilde{R}^*, \tag{3.7}$$

where an asterisk denotes transformed variables, for example

$$\tilde{\tau}^*(k, Y, t) = \int_{-\infty}^{\infty} \tilde{\tau}(X, Y, t)\,\mathrm{e}^{-\mathrm{i}kX}\,\mathrm{d}X. \tag{3.8}$$

Previous experience with this numerical technique suggests that a compressed/stretched grid in the Y-direction increases accuracy, and so a coordinate transformation

$$Y = f(\eta) \tag{3.9}$$

is made. It will be assumed that $0 \leqslant \eta < 1$ as $0 \leqslant Y < \infty$. Equation (3.7) then becomes

$$\frac{1}{\beta^2}\tilde{\tau}_t^* + \mathrm{i}kU_0\tilde{\tau}^* + \tau_{0Y}\tilde{V}^* - \frac{\tilde{\tau}_{\eta\eta}^*}{[f'(\eta)]^2} + \frac{f''(\eta)\,\tilde{\tau}_\eta^*}{[f'(\eta)]^3} = -\left[\tilde{U}\tilde{\tau}_X + \frac{\tilde{V}\tilde{\tau}_\eta}{f'(\eta)}\right]^* = \tilde{R}^*. \tag{3.10}$$

Equation (3.10) requires a knowledge of $\tilde{U}^*$ and $\tilde{V}^*$, and these are obtained as follows:

$$\tilde{U}^*(k, \eta, t) = \int_0^\eta f'(\eta_1)\,\tilde{\tau}^*(k, \eta_1, t)\,\mathrm{d}\eta_1, \tag{3.11}$$

$$\tilde{V}^*(k, \eta, t) = -\mathrm{i}k\int_0^\eta f'(\eta_2)\int_0^{\eta_2} f'(\eta_1)\,\tilde{\tau}^*(k, \eta_1, t)\,\mathrm{d}\eta_1\,\mathrm{d}\eta_2. \tag{3.12}$$

The Fourier transform of (3.6) is written symbolically as

$$P^* = \Lambda(k)\,A^*, \tag{3.13}$$

where (for example) $\Lambda(k) = -\mathrm{i}k$ for supersonic flows, (3.14)

and $\Lambda(k) = (k^2)^{\frac{1}{2}}$ for incompressible flows. (3.15)

for incompressible flows.

Combining the Fourier transforms of (3.5), (3.13) and the condition

$$\frac{\tilde{\tau}_\eta^*(\eta = 0)}{f'(0)} = \mathrm{i}k\tilde{P}^* \tag{3.16}$$

(which arises from the momentum equation (2.5) evaluated on $Y = 0$), results in a 'solubility' condition

$$\left.\frac{\tilde{\tau}_\eta^*}{f'(\eta)}\right|_{\eta=0} = \mathrm{i}k\Lambda(k)\left\{\left[\int_0^\eta f'(\eta_1)\,\tilde{\tau}^*(k, \eta_1, t)\,\mathrm{d}\eta_1\right]_{\eta\to 1} - hF^*\right\} \tag{3.17}$$

(as in I). The numerical scheme used in I was adopted, i.e. central differencing in η (grid size $\Delta\eta$), along with Crank–Nicolson marching in time (step size Δt) and

trapezoidal quadrature to treat the integrals in (3.11), (3.12) and (3.17). The scheme is overall second-order accurate in $\Delta\eta$ and Δt. Notice the useful property

$$\tilde{\tau}^*(-k,\eta,t) = \text{c.c.}\{\tilde{\tau}^*(k,\eta,t)\}, \tag{3.18}$$

which halves the domain that needs to be considered in k-space. $\frac{1}{2}K+1$ points in k-space were taken, from $k=-k_{\max}$ up to $k=0$, in steps of Δk.

The $\tilde{\tau}^*(0,\eta,t)$ were all set equal to zero at all times for all η. Although, for the limit $h\to 0$, this is a valid procedure, for $h=O(1)$ this amounts to imposing a slightly faster decay rate on the solution as $|X|\to\infty$ than is strictly the case. However this was found to contribute negligibly to the overall truncation error (as evidenced by comparing computations on grids of various Δk). The presence of the $\tau_{0Y}\tilde{V}^*$-term on the left-hand side of (3.10) has important repercussions. This was absent in I and the difference approximation resulted in a tridiagonal system (plus one full row) at each (k,t)-station. The additional term in (3.10) destroys this structure. If trapezoidal quadrature is used to evaluate $\tilde{V}^*$ from (3.12), then (symbolically)

$$\tilde{V}^*(k,j\Delta\eta,t) = (\Delta\eta)^2 \sum_{n=0}^{j}\sum_{m=0}^{n} \alpha_{n,m}\tilde{\tau}^*(k,m\Delta\eta,t) \tag{3.19}$$

(where the $\alpha_{n,m}$ are constants). The resulting set of difference equations at each (k,t)-station is then almost lower triangular (lower triangular with an additional band just above the diagonal). Simple Gaussian elimination procedures are still suitable for this system.

The overall technique was identical to that described in I (with the fast-Fourier transform of Cooley & Tukey 1965 being used in the nonlinear calculations to evaluate the right-hand side of (3.10)). Linearized results were obtained by setting $\tilde{R}^*\equiv 0$ in (3.10), and so required no iteration. For the transverse Y-transformation, as in I,

$$f(\eta) = \frac{\eta}{1-\eta} \tag{3.20}$$

was chosen, and (3.10) was solved over the range $0\leqslant\eta\leqslant 0.95$, spanned by J η-points, i.e. the transverse grid size $\Delta\eta = 0.95/(J-1)$.

The final point concerns the start-up procedure implemented. It was found that simply introducing the distortion into the undisturbed flow at some initial time ($t=t_s$, say), frequently caused the solution to 'ring', as might well be expected. Instead, a rather gentler start was given to the computation. This involved solving the quasi-steady form of (3.10) at $t=t_s$, with the time-derivative term $(1/\beta^2)\tilde{\tau}_t^*$ omitted. At the next time step ($t_s+\Delta t$), and subsequent time steps, the full equation (3.10) was solved, including the time-derivative term. This generally gave a very smooth start to the computation, as evidenced by comparing solutions at $t=t_s$ with those obtained exactly one cycle later at $t=t_s+2\pi$.

4. Results

Most computations were performed on a variety of numerical grids, which to a certain extent were chosen to match the particular distortion and set of physical parameters; the various grids uses are detailed in table 1. Generally, perturbation quantities will be presented, and so for reference figure 2 shows the variation of the unperturbed wall shear with time for a number of values of γ relevant to the following results ($\beta=1$ in all cases).

Grid	K	k_{max}	Δk	J	Δt
I	128	7.055	0.11	25	0.005
II	128	14.110	0.22	25	0.005
III	128	14.110	0.22	49	0.005
IV	64	7.111	0.22	25	0.005
V	256	7.027	0.055	25	0.005
VI	128	7.055	0.11	49	0.005
VII	64	7.111	0.22	49	0.005
VIII	128	14.110	0.22	25	0.0025
IX	256	14.055	0.11	25	0.005
X	256	28.110	0.22	25	0.005

TABLE 1. Grid parameters for the spectral method

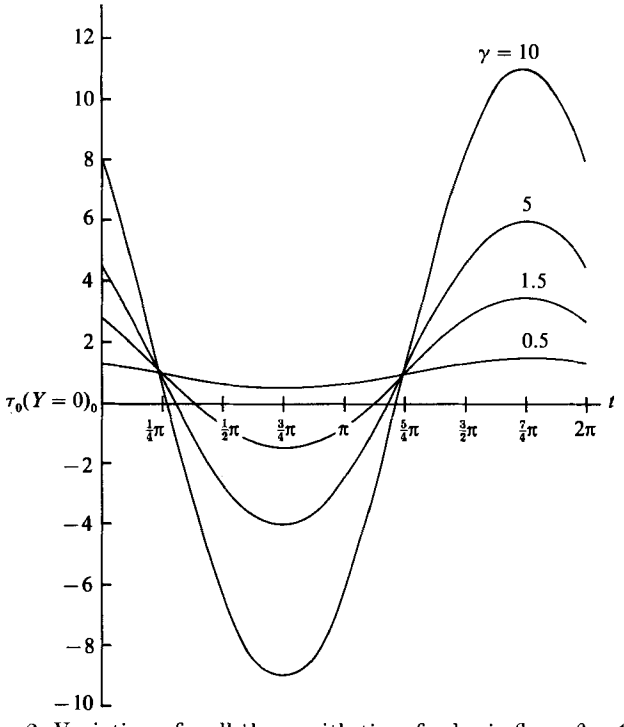

FIGURE 2. Variation of wall shear with time for basic flow, $\beta = 1$ in all cases.

Since analytic treatment of the governing system does not seem to be possible for the general linearized ($h \to 0$) case, numerical results of this class will also be presented; indeed it will be seen that even flows of this simplified type may exhibit certain interesting features.

4.1. *Linearized supersonic results*

The first problem considered pertains to the distortion

$$F(X) = \frac{1}{1+X^2}, \tag{4.1}$$

i.e.

$$F^*(k) = \pi e^{-|k|}, \tag{4.2}$$

with an amplitude parameter $\gamma = 2.5$ and a frequency parameter $\beta = 1$. The first set of results were obtained with a start-up time $t_s = -\frac{1}{2}\pi$, and were computed on grids I, II, III, IV, VIII and IX. All the results to be displayed are invariant with grid (to within graphical accuracy), except where stated. Temporal variations of perturbation wall shear ($\tilde{\tau}_w$) for this case are shown at four selected X-stations, namely $X = 0$, 2.5 (in figure 3a) and $X = 5$, 10 (in figure 3b).

The most striking feature of these distributions is the 'spiking' effect observed at downstream locations. In particular at $X = 5$ and 10, throughout much of the cycle the perturbation shear is of small amplitude; however, during certain periods of the cycle (the further downstream, the later the period) the wall shear (and indeed other physical quantities) suddenly grows in amplitude, oscillates and then decays away. This 'spiking' behaviour, whilst moving downstream with time, appears (by comparing the $X = 5$ and 10 results) to decay in amplitude, although temporally these oscillations become increasingly rapid. There was no discernible spiking effect upstream.

Figure 3(c, d) shows spatial distributions of perturbation wall shear at six selected times, deliberately chosen during the period of spiking as observed in figure 3(a, b), and the corresponding perturbation pressure distributions are shown in figure 3(e, f). These figures all confirm the downstream movement of the spikes, together with their ultimate decay and break-up downstream. Since the derivative of the displacement function is (minus) the pressure, the displacement function must also exhibit this behaviour.

It is revealing to inspect the behaviour of the solution in spectral (k) space during these periods of spiking. Figure 3(g) shows the spectral distribution of $\mathrm{Re}\{\tilde{\tau}_w^*\}$ at $t = 4.4242$ and for comparison the distribution at $t = 1.0492$ is shown on the same figure, a somewhat 'quieter' time during the cycle. (These distributions were obtained using grid III; other grids gave indistinguishable results on the scale shown, except grids I and IV of course, which truncated the spectral solution just beyond $k = -7$ but gave similar results up to the point of truncation.) Figure 3(h) shows the spectral distributions at two later times, namely $t = 6.3092$ and 8.3092, obtained on grid III, and are to be compared with figure 3(i), the results obtained on grid I. These figures indicate that at these later times large-amplitude oscillations are present in the spectral solution on grid I, which are however very much dependent on $\Delta\eta$ – a halving of this grid substantially reduces the amplitude of these oscillations. At the later time shown these oscillations have subsided considerably. The computation on grid VIII (not shown) revealed that a reduction in Δt had little effect on these oscillations. Interestingly, in spite of the difference in spectral solutions, the physical solutions at $t = 6.3092$ and 8.3092 obtained on grids I and III were graphically indistinguishable (see figure 3j). The control computation on grids II, IV (and IV) at $t = 6.3092$ did, however, produce oscillations in the physical solutions, well upstream of the distortion ($X = 0$), which travelled downstream, decaying in the process, and were not noticeable at $X = 0$. These oscillations were insignificant in the computations with smaller Δk (grids I, IX), or smaller $\Delta\eta$ (grid III). Presumably, although the smaller-Δk results still possess oscillations in k-space, the effect is fortuitously self-cancelling. From the evidence above, in particular their demise in physical space with a refinement of the k- or η-grids, these oscillations in physical quantities are likely to be spurious, caused through too coarse a numerical grid.

The physical processes responsible for the spiking phenomenon found during periods of the cycle are of interest. Figures 3(k), 3(l) and 3(m) show the instantaneous streamline patterns at $t = 3.1542$, 3.5442 and 4.0592 respectively (these times

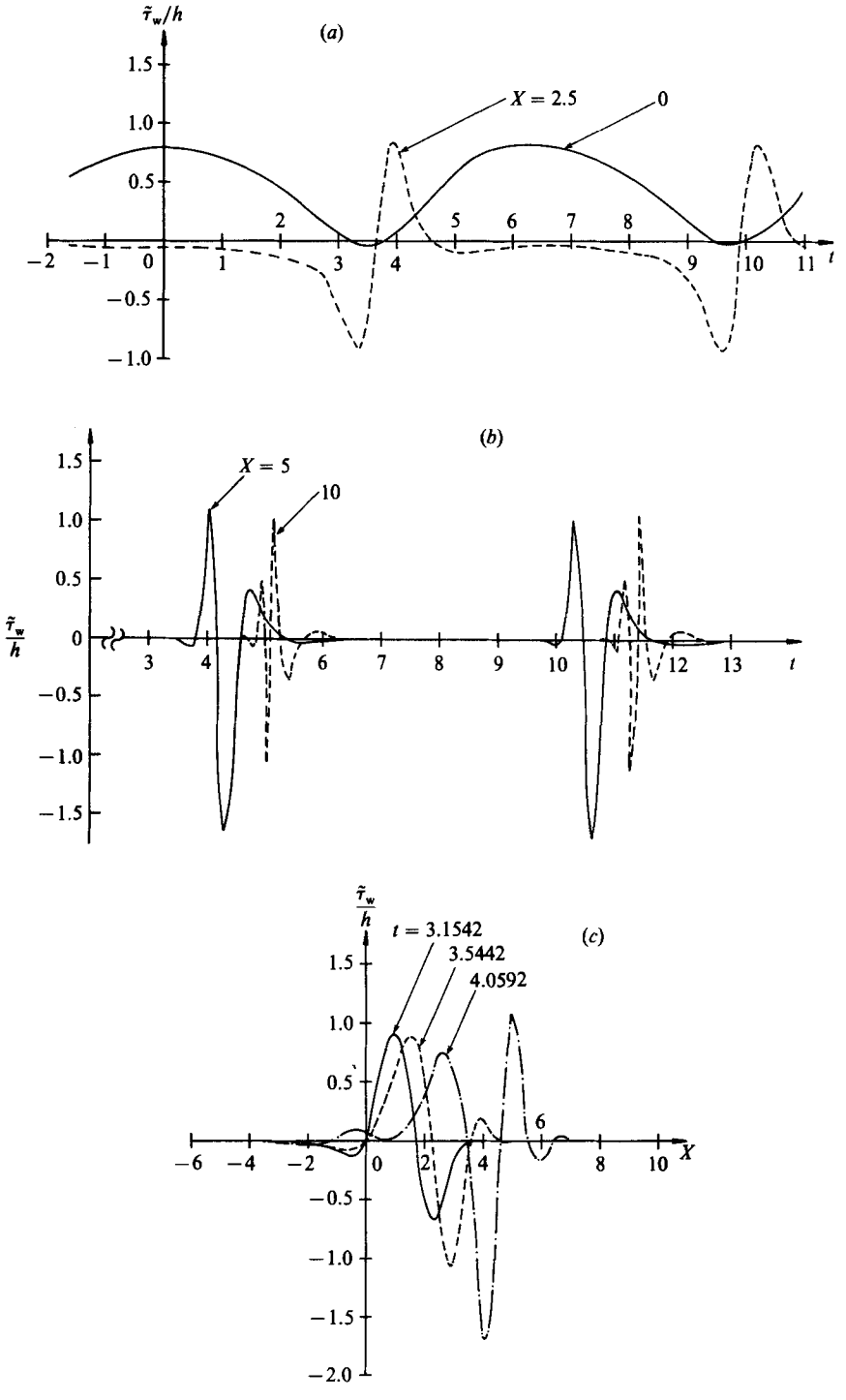

FIGURE 3(*a–c*). For caption see p. 273.

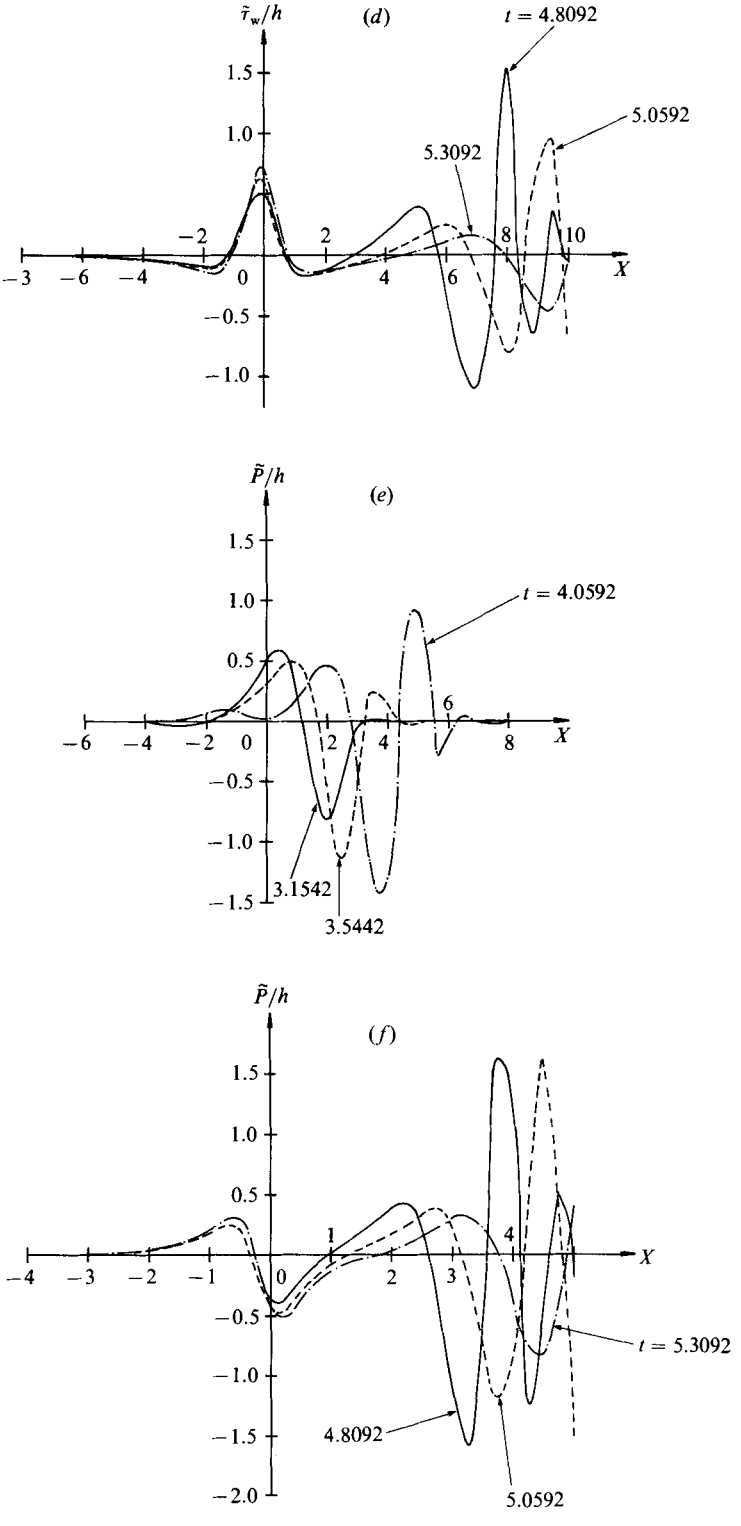

FIGURE 3(*d–f*). For caption see p. 273.

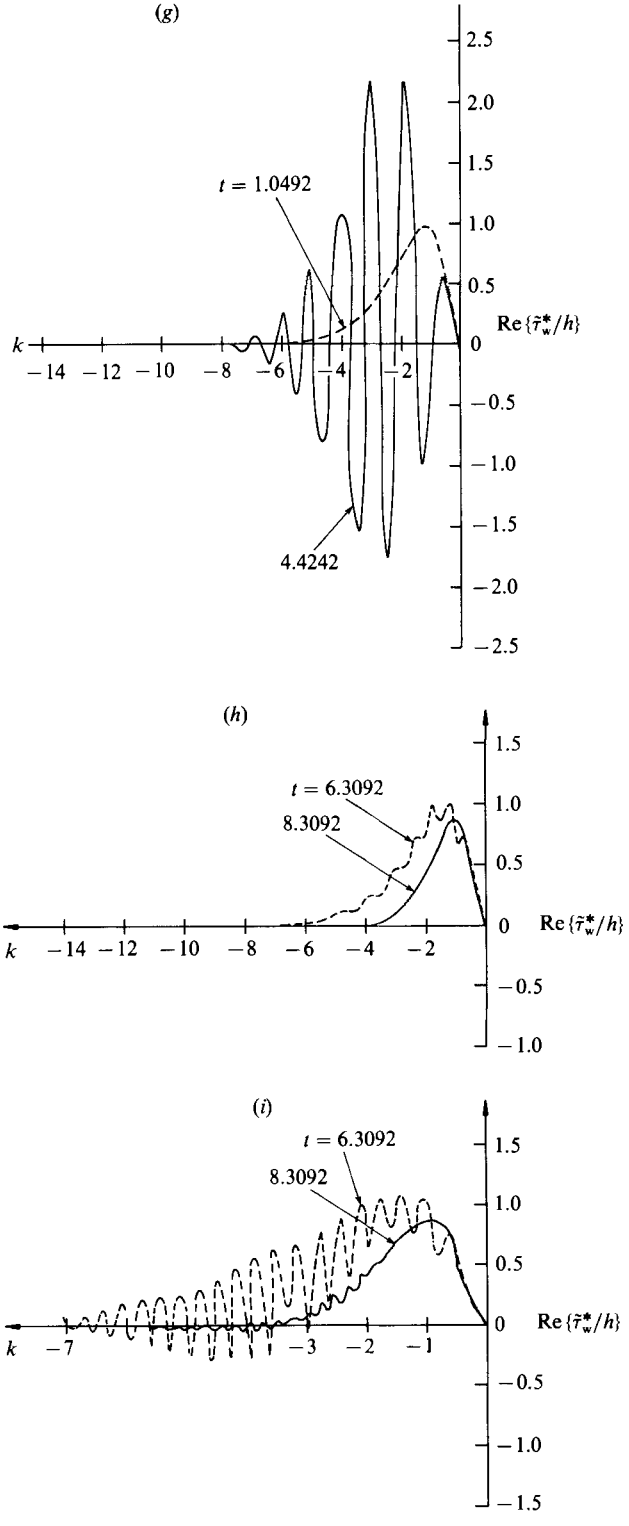

FIGURE 3(*g–i*). For caption see p. 273.

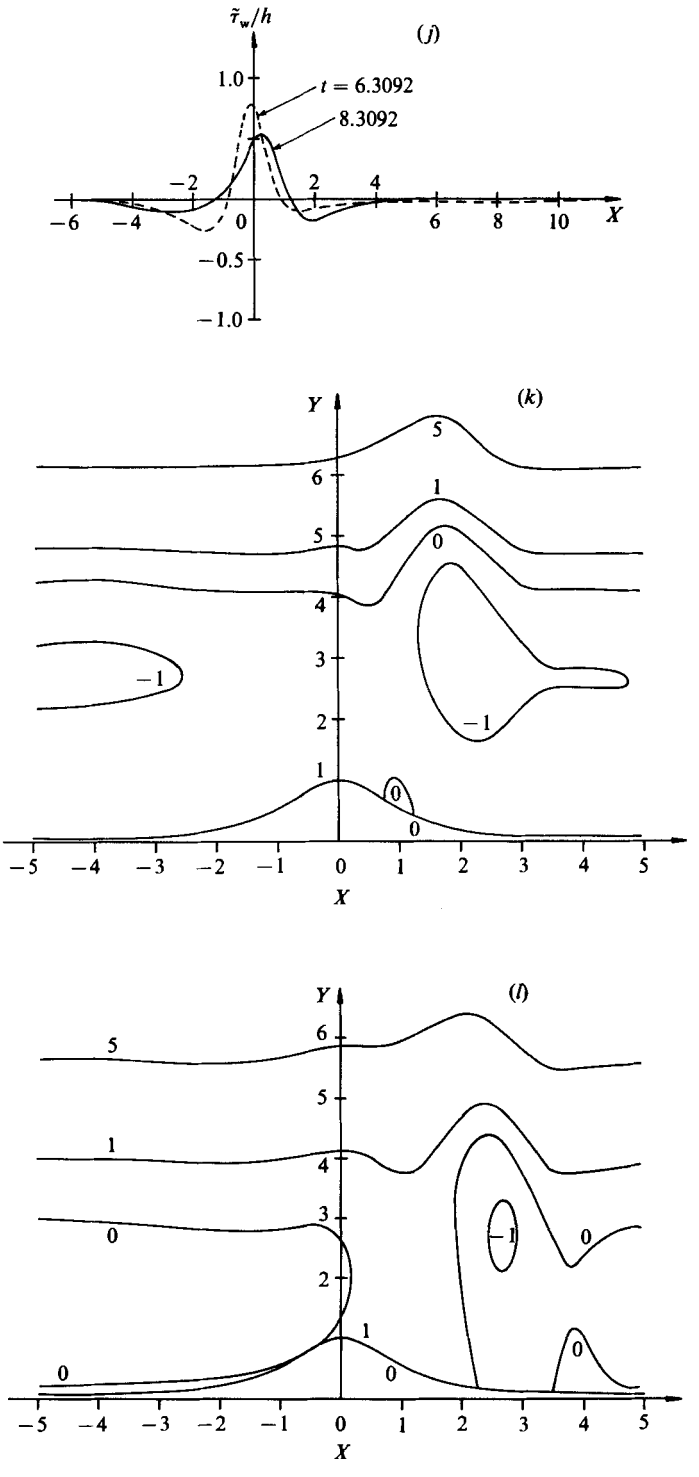

FIGURE 3 (*j–l*). For caption see facing page.

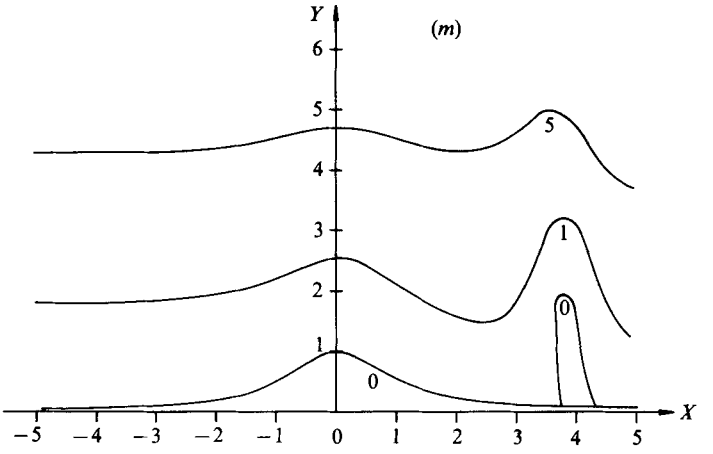

FIGURE 3. (a,b) Temporal variation of perturbation wall shear at fixed locations (as indicated); (c,d) distribution of perturbation wall shear; (e,f) distribution of perturbation pressure; (g,h,i) spectral distribution of Re $(\tilde{\tau}_w^*)/h$; (j) distribution of perturbation wall shear; (k,l,m) instantaneous streamlines at $t = 3.1542$, 3.5442 and 4.0592 respectively. Supersonic linear case; $\gamma = 2.5$, $t_s = \frac{1}{2}\pi$, $\beta = 1$, profile (4.1), grid III (grid I for i).

corresponding to those chosen in figures 3*c*, 3*e*). Since these are linearized results, here a height parameter of $h = 1$ is taken. (These streamlines were obtained by using a second-order interpolation routine in (X,η)-space on the grid III results.)

The most startling feature of the streamline pattern is the presence of so-called 'cats-eye' eddies in the main body of the boundary layer (see for example Sobey 1980, 1982, 1985).† Important physical processes are thus likely to be occurring away from the wall. Figures 3 (*k–m*) span the period of time during which the undisturbed flow reverses at the wall (for this particular choice of parameters reversal at the wall occurs at $t \approx 3.5154$), which seems to be a critical time for the flow. The region of reversed flow moves downstream and subsides as time progresses, and indeed coincides with the spiking effect observed in the wall shear the pressure distributions. One possible explanation of this effect is the onset of a Rayleigh (large-wavenumber) instability (cf. Smith & Bodonyi 1985; Tutty & Cowley 1986). Instabilities of this class are well known to be linked to inflexional-type velocity profiles, and the profile (2.9) has an infinite number of inflexion points at all times, for all values of γ and β.

Following Smith & Bodonyi (1985) and Tutty & Cowley (1986), large-wavenumber ($|k| \to \infty$) instabilities may exist with temporal growth rates $c_i = O(k)$. (The former authors considered a streamwise lengthscale shorter than that of the triple deck, whilst the latter authors emphasized the triple-deck formulation; however the two approaches do match.) The multiple scales analysis of these previous authors is applicable to the basic profile (2.9), and figure 4 shows the variation of c_i with t (which appears as a parameter in this context) for the case $\gamma = 2.5$, $\beta = 1$. These computations were performed using the method of Tutty & Cowley (1986), using a program kindly supplied by them. (Note that this distribution of $c_i(t)$, and those shown later are completely independent of the distortion height or shape, and depend

† The streamline patterns presented by Tutty & Cowley (1986) do not correspond to the actual streamlines, but rather to the values of the 'Prandtl transformed' streamlines; since the wall distortion is moving transversely in their case, the wall itself does not coincide with a streamline.

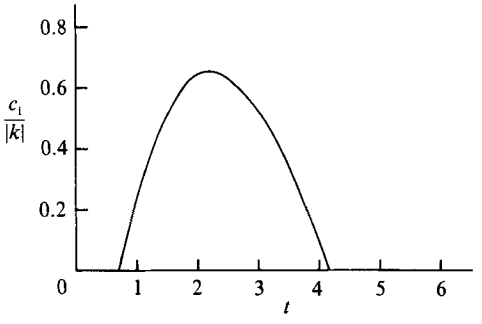

FIGURE 4. Growth rate for Rayleigh instability; $\gamma = 2.5$, $\beta = 1$.

only on the flow parameters γ and β.) Figure 4 indicates that instabilities of the Rayleigh type can appear during the cycle, although the author was unable to find solutions at all times. Further, there does seem to be some correlation between the presence and growth of the spiking, and the existence of solutions to the Rayleigh problem (in fact the correlation is somewhat stronger with the integrated growth rate).

Computing times for this problem were fairly lengthy – a computation using grid I took approximately 20 minutes on a CDC 7600 to advance 5 units in t. Computational times on other grids may be estimated using this figure as a basis, and noting that the largest component of the solution process for these linear examples is the Gaussian elimination process, which requires $O(J^2K)$ operations (this is in contrast to I, where the solution of the tridiagonal system at each (t, k)-station involved $O(JK)$ operations).

A final comment regarding this particular example concerns the choice of start-up process. This works very well in the current examples as evidenced by comparing quantities 2π apart in t in figures 3 (a) and 3 (b) (although the further downstream, the more time is necessary for periodicity to develop).

The above example was repeated on grids I, II, III, IV, VIII, IX and X, but with $t_s = 0$, instead of $-\frac{1}{2}\pi$. At early times all these computations produced results very close to the $t_s = -\frac{1}{2}\pi$ results. However by $t \approx 3.6$ the spectral solution on grids I, III and VIII had in all cases ceased to decay for $|k| \gg 1$. In the case of grid X (the grid with the largest k-range), this exhibited $|k| \gg 1$ growth by $t = 3.1$. Varying $\Delta\eta$ and Δt had negligible effect. The distribution of $\mathrm{Re}\{\tilde{\tau}_w^*\}$ (which is typical of all spectral distributions) at $t = 4.38$, obtained on grid II is shown in figure 5. The growth in the spectral solution for $|k| \gg 1$ was mirrored in the physical solution by increasing-amplitude oscillations (both spatial and temporal) downstream of the distortion, which were grid sensitive. The results in figure 5 are well after the period of time during which the physical results may be considered reliable.

It is curious that starting the same computation at a later time can cause such a profound difference to the solution, even though the solutions initially are so close. A possible explanation for this can be found from the discussion earlier of the large-wavenumber, Rayleigh instability. Figure 4 indicates that $|k| \gg 1$ disturbances exhibit growth (in the particular case of $\gamma = 2.5$, $\beta = 1$) from $t \approx 0.75$ until $t \approx 4.15$. Outside this interval, such disturbances may decay. Consequently in the case of the $t_s = 0$ computations large-wavenumber disturbances (in particular those caused by the start-up process) soon enter a period of growth, (after approximately 0.75 time units) whilst in the case of the $t_s = -\frac{1}{2}\pi$ computations, disturbances are not subject

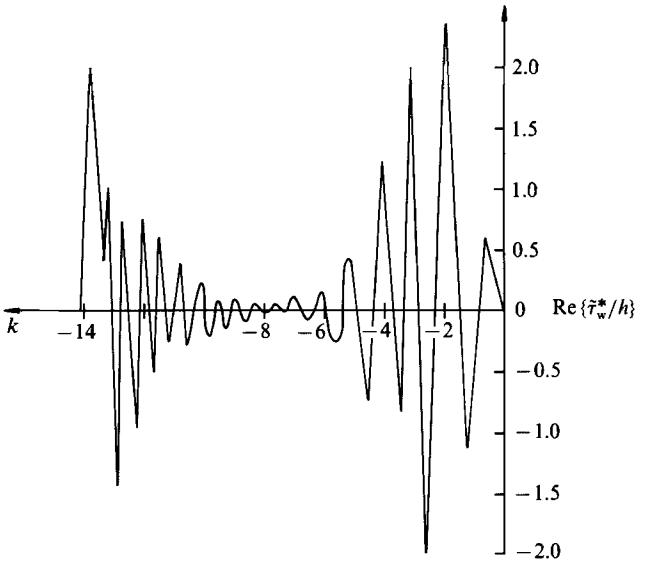

FIGURE 5. Spectral distribution of Re$\{\tilde{\tau}_w^*/h\}$. Details as for figure 3 except grid II, $t_s = 0$.

to growth until approximately 2.32 units of time have elapsed. This could conceivably account for the discrepancy between the results for the two starting times.

The use of a less extensive k-range (e.g. grid I), with $t_s = 0$ actually sidesteps this problem, giving results that compare very favourably with the $t_s = -\frac{1}{2}\pi$ results at all times; however the use of this technique for overcoming the problem cannot be properly justified.

The next example for which results are presented is the case $\gamma = 5$, $\beta = 1$, taking again the distortion profile (4.1). Results (obtained on grid III), using a starting time $t_s = -\frac{1}{2}\pi$ are shown in figure 6. Shortly after the latest time shown ($t = 2.3742$) the (physical) wall shear grew increasingly rapidly with t, especially around $X = 1$ (figure 6*a*); the perturbation pressure distributions are shown in figure 6(*b*). The corresponding distribution of Re$\{\tilde{\tau}_w^*\}$ with k is shown in figure 6(*c*), and this indicates a deterioration of decay of the spectral solution with k. Taken together, the physical and spectral trends all point to a singularity developing in the solution, although the results after $t = 2.3742$ were deemed unreliable because of the poor decay of the spectral solution as $|k| \to \infty$.

This calculation was checked using grids I, II and VIII. The solutions obtained on grids I and VII were indistinguishable from the grid-III results shown in figure 6; the grid-II results did differ at $t = 2.3742$, owing to oscillations downstream of $X = 1$. These effects may well be caused by the truncated k-range used by grid II, which figure 5(*c*) shows could be significant.

The calculation was repeated on grids I, II, III and IV, using $t_s = 0$. The previous distributions (obtained using $t_s = -\frac{1}{2}\pi$) were confirmed to within the graphical accuracy of figure 6. In particular the suggestion that a singularity was developing sometime after $t = 2.3742$ was confirmed.

A search was made for $|k| \gg 1$ Rayleigh modes of instability for $\gamma = 5$, $\beta = 1$, and results for the growth rate c_i are presented in figure 7. This reveals that unstable Rayleigh modes are present through much of the cycle, with the amplitude of the growth rate approximately double that obtained for $\gamma = 2.5$ (figure 4). Indeed we expect more instability as γ increases (as the velocity profile becomes more like a

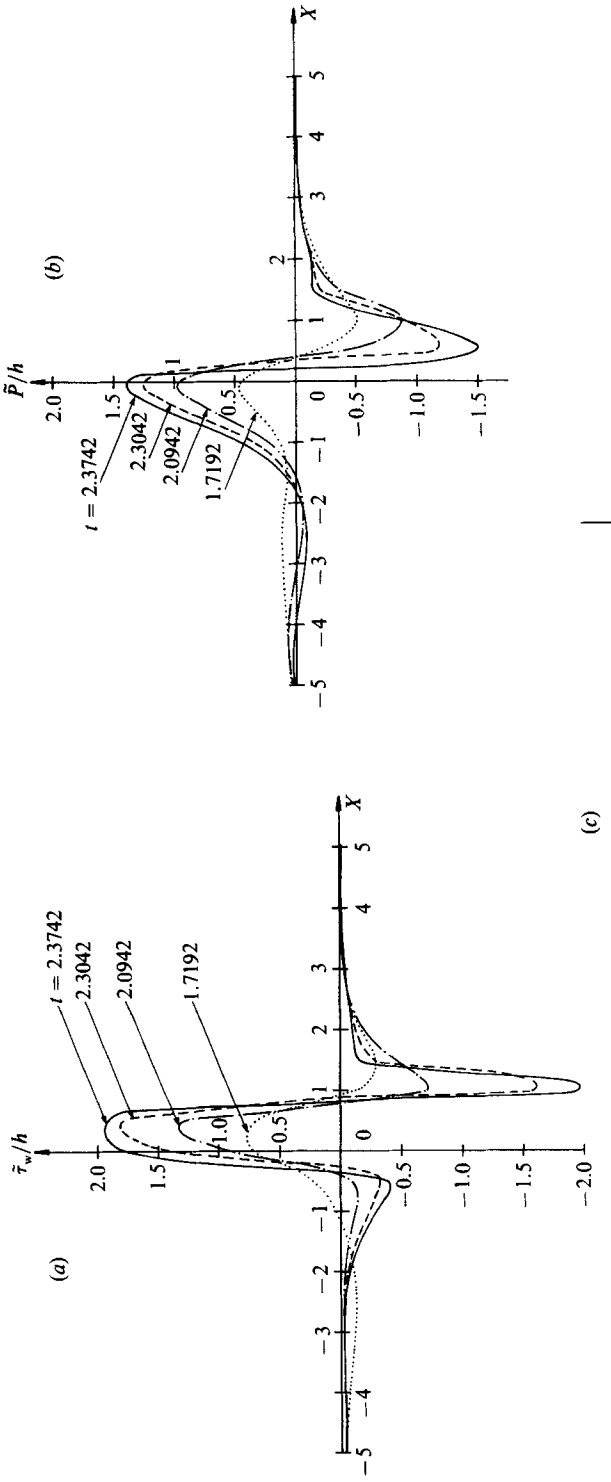

FIGURE 6. (*a*) Distribution of perturbation wall shear; (*b*) distribution of perturbation pressure; (*c*) spectral distribution of $\mathrm{Re}\,(\tilde{\tau}_w^*)/h$. Supersonic linear case, $\gamma = 5$, $t_s = -\frac{1}{2}\pi$, $\beta = 1$, profile (4.1), grid III.

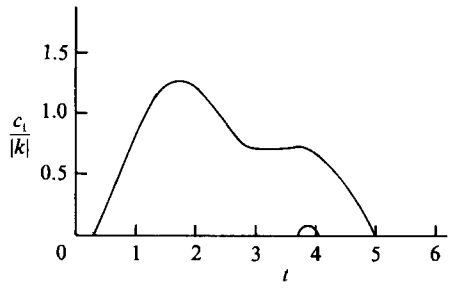

FIGURE 7. Growth rate for Rayleigh instability; $\gamma = 5$, $\beta = 1$.

Stokes layer). Interestingly, for $\gamma = 5$, a small, secondary mode is also seen to occur, between $t \approx 3.7$ and $t \approx 4.1$.

The increased growth rates, together with the increased period that Raleigh instability is present could well explain why in this case the solution seems to break down both for $t_s = -\frac{1}{2}\pi$ and $t_s = 0$. This is similar in some respects to the suggested breakdown in I, Duck (1985*b*) and Tutty & Cowley (1986), which also seem to be linked to $|k| \gg 1$ growth.

However, there is an important distinction between the present results and those of previous works in so far as here the singularity must be linear, whilst the previous cases mentioned above were all nonlinear examples (although in a similar nonlinear system, Brotherton–Ratcliffe & Smith 1987 have shown how the flow can break down in a basically linear manner). These results suggest no periodic solution exists for this particular configuration (within the restriction of the triple-deck model). Inspection of the streamlines for $\gamma = 5$ (with a notional value of $h = 1$) prior to the apparent breakdown (not shown) again reveals a flow pattern similar to that found in figure 3(*k–m*) including 'cats-eye' eddies.

As a final supersonic linearized example the alternative distortion profile was taken, namely

$$F(X) = \mathrm{e}^{-\frac{1}{4}X^2}, \tag{4.3}$$

for which

$$F^*(k) = 2\pi^{\frac{1}{2}}\mathrm{e}^{-k^2}. \tag{4.4}$$

The motivation in choosing this shape is to investigate if a more rapid decay of $F^*(k)$ with k can delay (or even eradicate) some of the effects observed in the previous examples. This seems to be the case, as illustrated in figure 8 where results for $\gamma = 10$, $\beta = 1$, $t_s = 0$ are presented. These results were obtained with grid V and checked by computations on grids I, II and VI. There is no sign of the breakdown suggested in a number of the previous computations, and reasonable periodicity seems to have been established in t. Figure 8(*b*) shows the downstream movement of the spiking whilst figure 8(*a*) indicates that a similar spiking behaviour is beginning to occur upstream of the distortion (and moving upstream); the latter is found at $t \approx 2.5$, and the former at $t \approx 4.5$. It is to be expected that as γ increases (provided periodic solutions exist) conditions upstream, close to the wall, will become progressively like the reflection of those downstream close to the wall, at a time π earlier/later. A further trend to be expected (and observed) is that the speed these spikes propagate upstream/downstream increases as γ increases.

Figure 8(*c*) shows the growth rates of Rayleigh mode instabilities throughout the cycle. Secondary modes are seen to be present during two time periods; the primary

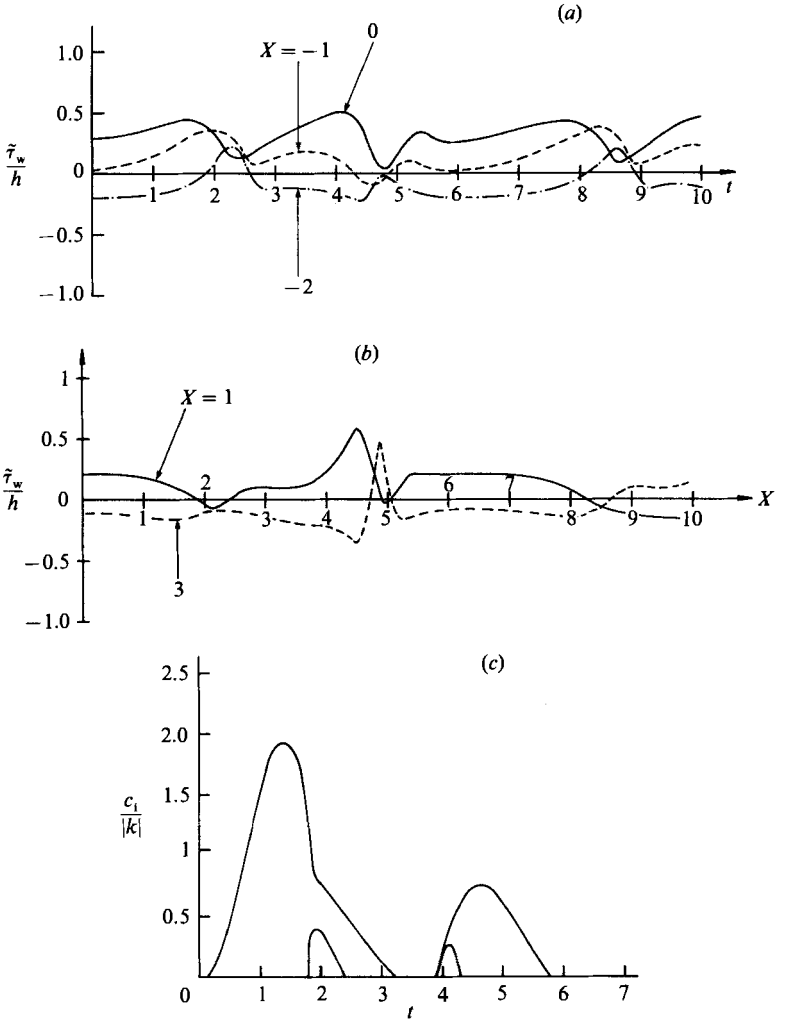

FIGURE 8. (a, b) Temporal variation of perturbation wall shear at fixed X-locations (as indicated); supersonic linear case, $\gamma = 10$, $t_s = 0$, b = 1, profile (4.3), grid V. (c) Growth rate for Rayleigh instability; $\gamma = 10$, $\beta = 1$.

instability has split into two distinct distributions, presumably corresponding to upstream- and downstream-moving spikes.

The following section considers solutions of the nonlinear supersonic problem.

4.2. *Nonlinear supersonic results*

The first set of results to be presented for this class is for the flow over profile (4.1), with $\gamma = 2.5$, $\beta = 1$ and $h = 1$ (a hump type of distortion). This example is the nonlinear counterpart of the first case considered in §4.1, and so direct comparison may be made to judge the effects of nonlinearity.

Figures $9(a, b)$ show distributions of perturbation wall shear and pressure respectively, obtained using grid II and $t_s = 0$. These results point to the likely development of some form of singularity, close to $X = 2.5$, shortly after $t = 3.255$. Figure $9(c)$ shows the (spectral) distribution of $\mathrm{Re}\,[\tilde{\tau}_w^*]$ at $t = 2.63$ and 3.225, and this indicates that the growth in certain regions of the physical $\tilde{\tau}_w$ solution is mirrored in

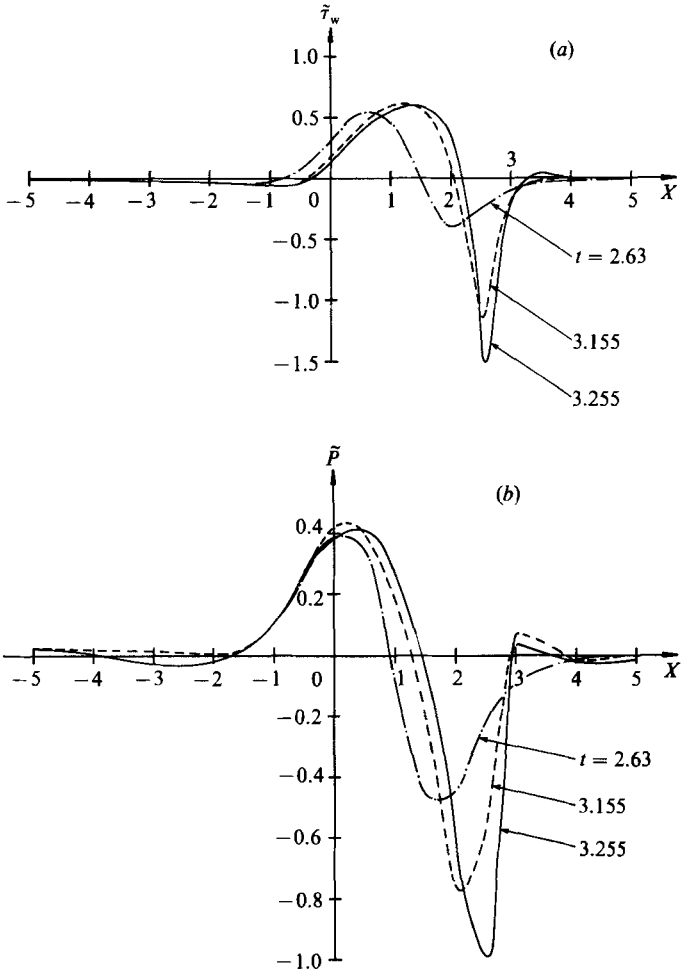

FIGURE 9(*a*, *b*). For caption see p. 281.

spectral space by a growth in $|k| \gg 1$ modes. By comparison with the linear distributions of figure 3(*g*), nonlinearity is seen to enhance the growth of these modes, leading to an apparent singularity in the physical solution. The computation was abandoned after $t = 3.255$, owing to lack of adequate decay of the spectral solutions for $|k| \gg 1$. The calculation for this case was repeated using grids III, IV and VIII, which substantiate the accuracy of the figures (although after $t = 3.255$ discrepancies did become apparent).

Because of the discrepancy between the $t_s = 0$ and $t_s = -\frac{1}{2}\pi$ linear solutions for this choice of γ and β, a calculation was performed with $t_s = -\frac{1}{2}\pi$, on grid II; this seemed to develop a singularity at the same time and location as the $t_s = 0$ computations described above.

Figure 9(*d–f*) shows the streamlines for this case (obtained on grid III with $t_s = 0$). The 'cats-eye' pattern is again observed (just prior to the breakdown of the solution), which seems to induce the large streamwise pressure gradient which in turn causes the rapid growth in wall shear. Overall, nonlinearity hastens the onset of the $|k| \gg 1$ growth in this instance.

Computations of this type were lengthy. Typically for this case, grid-II calculations

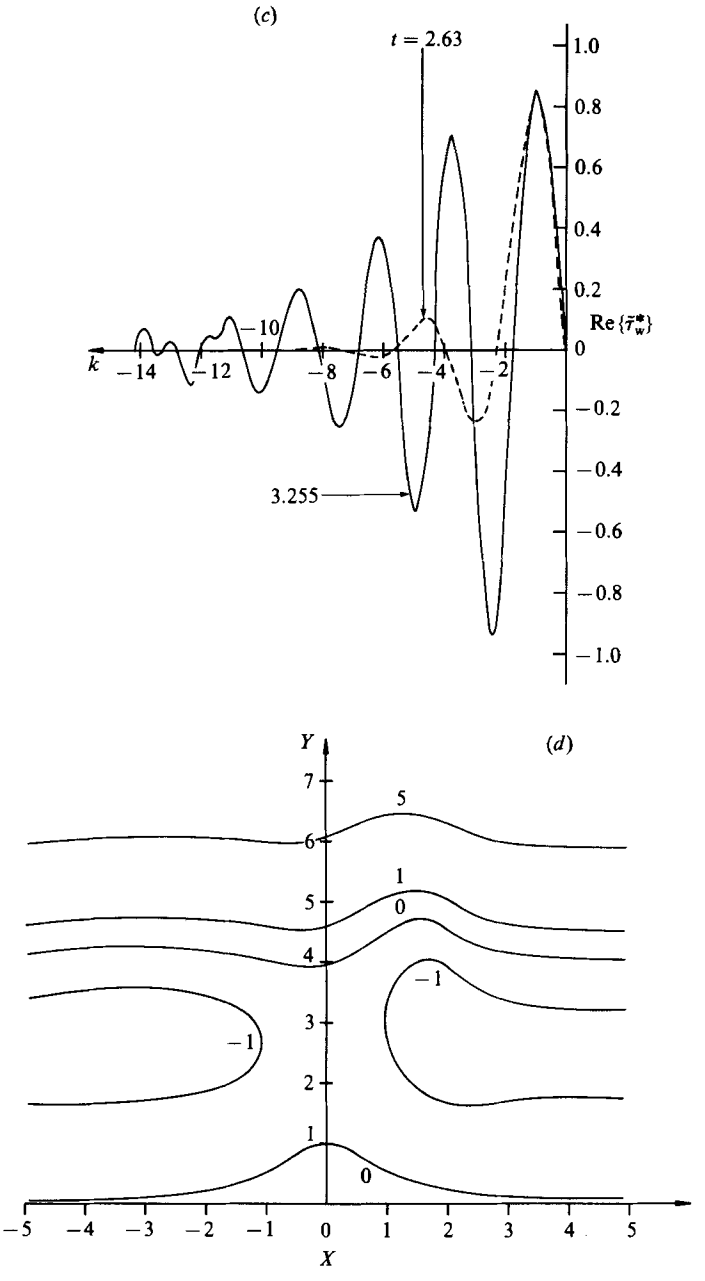

FIGURE 9(*c*, *d*). For caption see facing page.

took approximately 40 minutes of CDC 7600 time to advance the solution one unit in t.

Figure 10(*a*) shows the distribution of perturbation wall shear for the case $\gamma = 2.5$, $\beta = 1$, profile (4.1), with $h = -1$ (a hollow type of distortion), obtained using grid II with $t_s = 0$. Again it appears that a singularity is forming, mirrored by a rapid growth in the spectral variables for $|k| \gg 1$. In this case, the growth was somewhat slower than the corresponding $h = 1$ example (although these effects seem to be occurring at about the same time in both cases, just prior to the time of reversal of

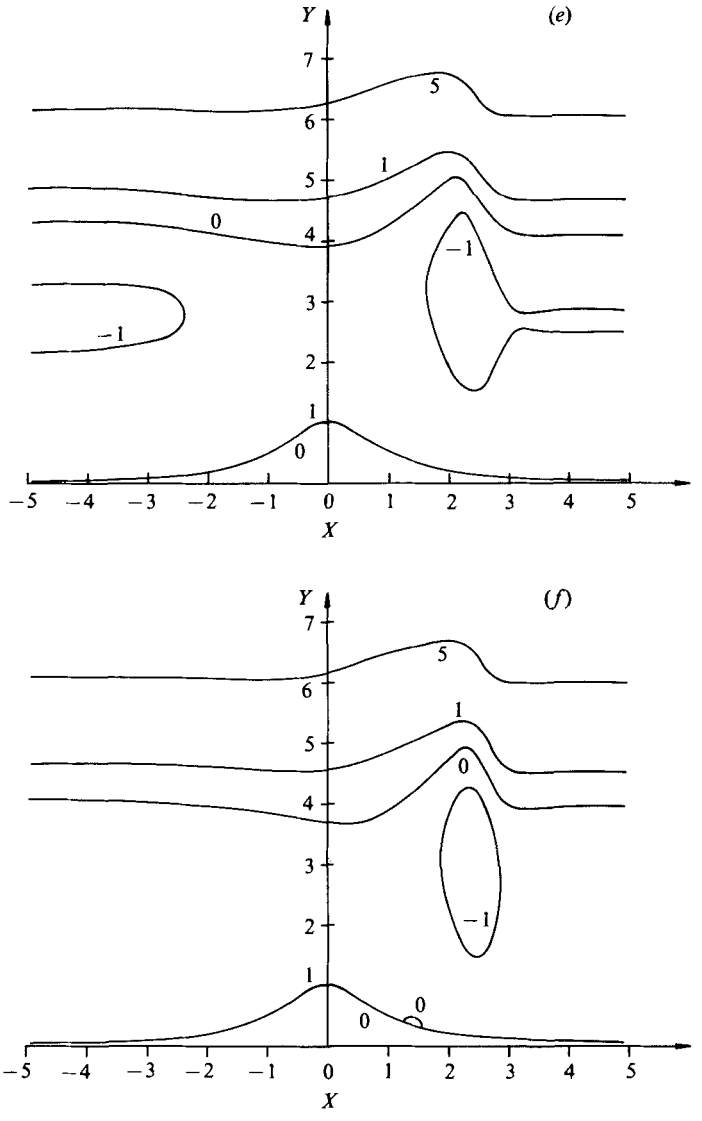

FIGURE 9. (*a*) Distribution of perturbation wall shear; (*b*) distribution of perturbation pressure; (*c*) spectral distribution of $\mathrm{Re}(\tilde{\tau}_w^*)$; (*d–f*) instantaneous streamline pattern at $t = 2.63$, 3.155, 3.255 respectively. Supersonic nonlinear case; $\gamma = 2.5$, $t_s = 0$, $\beta = 1$, $h = 1$, profile (4.1), (*a–c*) grid II (*d–f*) grid III.

the undisturbed flow at the wall), but further upstream ($X \approx 1$) in the case of a hollow distortion. The instantaneous streamline patterns at the three times shown in figure 9(*a*) are presented in figure 10(*b–d*). Again, the apparent breakdown is proceeded by the formation of 'cats-eye' eddies, away from the surface.

A computation was performed on the example $\gamma = 5$, $\beta = 1$, profile (4.1) with $h = 1$ using $t_s = 0$ and grid IV, corresponding to the second example considered in §2.1. Results are not presented for this case, since the apparent breakdown was very similar in nature to the corresponding linearized example, although at a slightly earlier time (shortly after $t = 1.9$) indicating again that nonlinearity enhances large-wavenumber mode growth (in this case). Further evidence of this was provided by

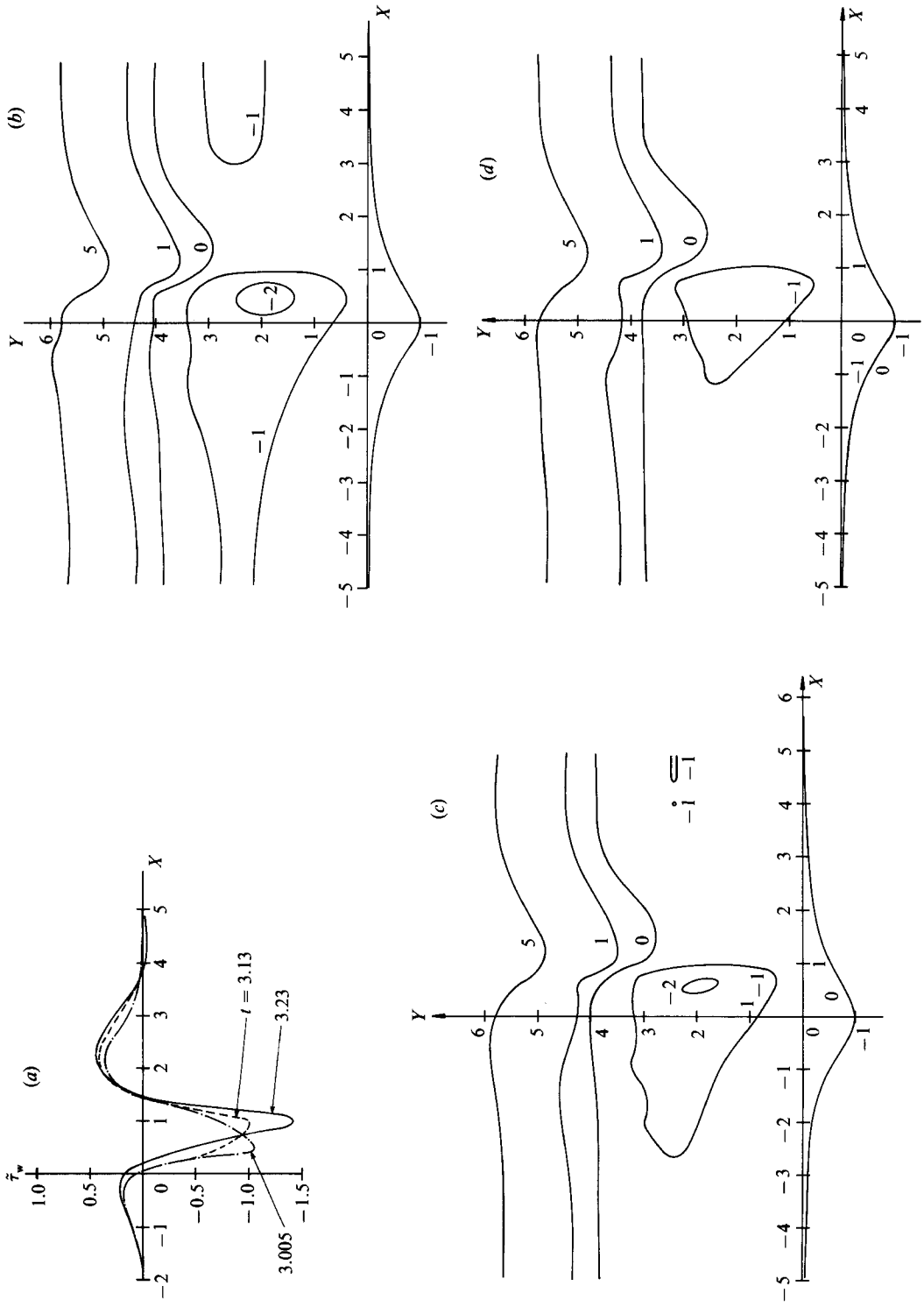

FIGURE 10. (*a*) Distribution of perturbation wall shear. (*b, c, d*) Instantaneous streamline pattern at $t = 3.005$, 3.13, 3.23 respectively. Details as for figure 9, but with $h = -1$, grid II.

the example of $\gamma = 5$, $\beta = 1$, $h = 1$, and profile (4.3) using $t_s = 0$ (results of which are also not presented here), which developed $|k| \gg 1$ growth (in much the same manner as observed in the previous examples) around $t = 3$, and mirrored by a rapid growth of a section of the physical wall shear. This is in contrast to the corresponding linearized example which attained temporal periodicity.

To conclude this subsection the solution in the limit of increasingly fast oscillations, i.e. $\beta \to 0$, is developed and comparison will be made with numerical results. (The limit $\gamma \to 0$ is of course a trivial limit, corresponding to the steady solution.)

The solution of (2.5) and (2.6) as $\beta \to 0$, for $Y = O(1)$ (guided by the results of Duck 1978, 1980, 1981), develops as

$$U = \gamma \cos t + U_0^{(s)}(X, Y) + O(\beta^2), \tag{4.5}$$

$$V = V_0^{(s)}(X, Y) + O(\beta^2), \tag{4.6}$$

$$P = \frac{\gamma X \sin t}{\beta^2} + P_0^{(s)}(X) + O(\beta^2), \tag{4.7}$$

$$A = A_0^{(s)}(X) + O(\beta^2), \tag{4.8}$$

where

$$U_0^{(s)} U_{0X}^{(s)} + V_0^{(s)} U_{0Y}^{(s)} = U_{YY}^{(s)} - P_{0X}^{(s)}(X), \tag{4.9}$$

$$U_{0X}^{(s)} + V_{0Y}^{(s)} = 0. \tag{4.10}$$

Here

$$U_0^{(s)} = V_0^{(s)} = 0 \quad \text{on} \quad Y = 0, \tag{4.11}$$

and

$$U_0^{(s)} \to Y + hF(X) + A_0^{(s)}(X), \tag{4.12}$$

$$P_0^{(s)}(X) = -A_{0X}^{(s)}(X). \tag{4.13}$$

Quantities with a superscript (s) refer to steady quantities, and these turn out to be identical to the steady ($\gamma = 0$) solution. In deriving the above, the no-slip condition on $Y = 0$ has been relaxed on the unsteady component of the flow. However this is resolved by introducing a thin (Stokes) layer, wherein $\tilde{Y} = Y/\beta = O(1)$, and

$$U = U_0^{(u)}(\tilde{Y}, t) + \beta U_{0Y}^{(s)}(X, 0)\, \tilde{Y} + O(\beta^2), \tag{4.14}$$

$$V = O(\beta^2). \tag{4.15}$$

$U_0^{(u)}$ is the Stokes solution, viz.

$$U_0^{(u)} = \tfrac{1}{2}\gamma[1 - e^{-(1+i)\tilde{Y}/\sqrt{2}}]\, e^{it} + \text{c.c.} \tag{4.16}$$

The implication of this is that the perturbation quantities, as computed in the numerical scheme, $\tilde{\tau}(X, Y, t)$ and $\tilde{P}(X, t)$ should approach $U_{0Y}^{(s)}(X, Y)$ and $P_0^{(s)}(X)$ respectively, as $\beta \to 0$.

Figure 11 (*a*) shows the temporal variation of the wall shear $\tilde{\tau}_w(X = 0, t)$ for the case $\gamma = 0.5$, $h = 1$, profile (4.1), for both $\beta = 0.5$ and 0.25; the steady value is also indicated on the figure (all results were obtained on grid I). There was no sign of any breakdown (observed in a number of the previous computations). There is a clear indication of the solution approaching the steady value as $\beta \to 0$. Further evidence of this trend is provided by figure 11 (*b*), comparing the spatial distributions of $\tilde{\tau}_w$ at $t = 6.1$ for the above two values of β, with the steady distribution.

4.3. *Linearized incompressible results*

From I it is to be expected that accurate incompressible calculations are a good deal more difficult to produce numerically than their supersonic counterparts, owing to

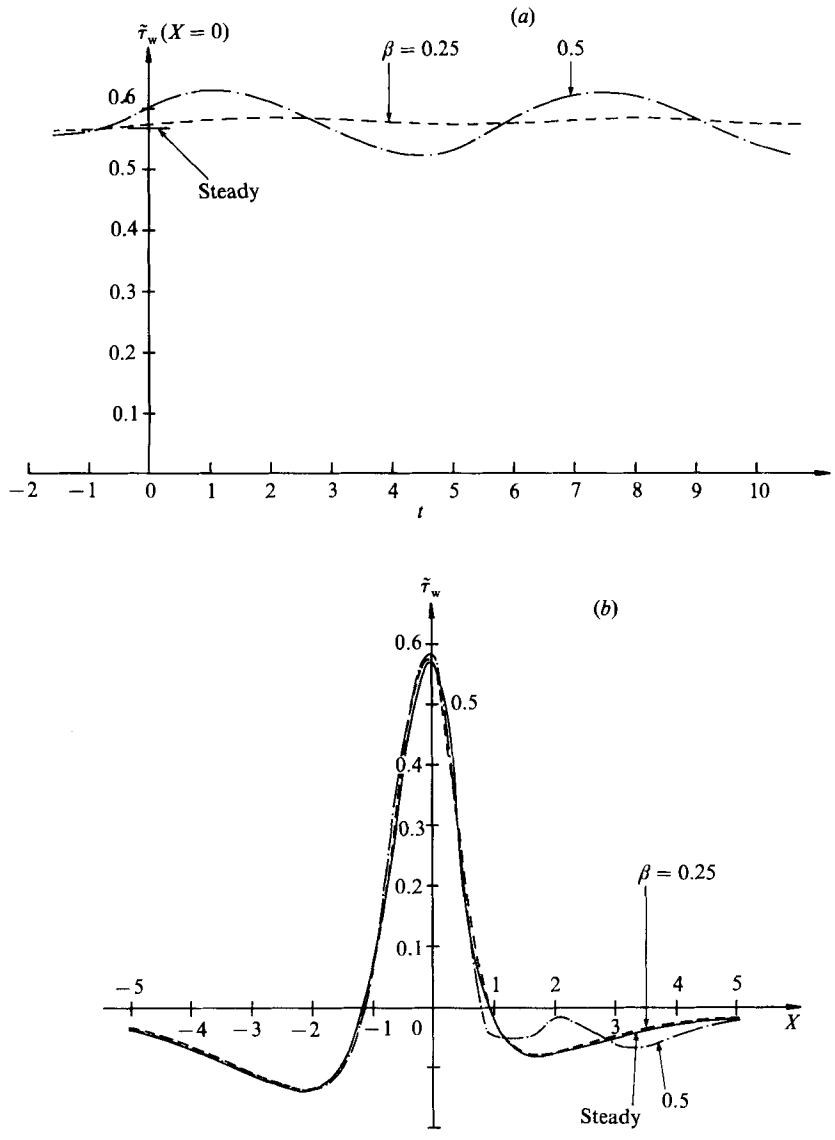

FIGURE 11. (*a*) Temporal variation of perturbation wall shear at $X = 0$, $\beta = 0.5$ and $\beta = 0.25$ (nonlinear cases) and comparison with steady value. (*b*) Comparison of spatial distributions of perturbation wall shear for $h = 1$, steady case with $\gamma = 1$, $\beta = 0.25$ and $\beta = 0.5$.

the presence of the Tollmien–Schlichting mode of instability. Indeed, it was found in I that the operation of starting the motion triggered unstable Tollmien–Schlichting modes, and caused a growing wave packet to be transmitted downstream. These instabilities revealed themselves numerically as increasingly large-amplitude oscillations in spectral space (with the largest growth rate at a finite value of k). These oscillations in turn eventually caused the breakdown of the solution (although in the linearized case this could be controlled by reducing Δk).

In the present study involving pulsatile boundary layers, it is to be expected that growing Tollmien–Schlichting instabilities will always be present, even in fully developed, time-periodic solutions, however small γ, because the unsteady nature

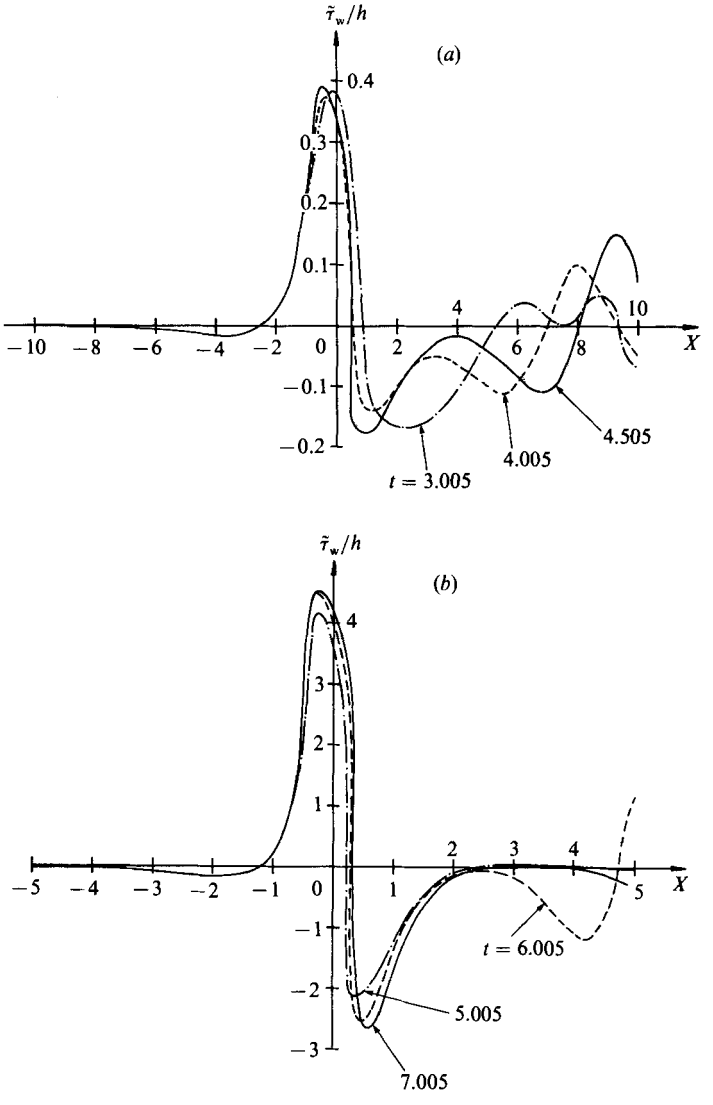

FIGURE 12. (*a*, *b*) Distribution of perturbation wall shear; incompressible, linear case, $\gamma = 0.5$, $t_s = 0$, $\beta = 1$, profile (4.1), grid V.

of the main flow causes a cascade process, triggering all time modes, most of which will be unstable.

The first example here is the flow over distortion profile (4.1), with $\gamma = 0.5$, $\beta = 1$. Perturbation wall shear distributions obtained on grid V (with $t_s = 0$) are shown in figure 12(*a*, *b*). This figure indicates that Tollmien–Schlichting waves are being formed which grow downstream. However after $t \approx 6$, over the range of X shown, this process stops, and no waves are generated. Unfortunately this calculation became unreliable (in the manner found in I and described above) after $t \approx 8$ (a control computation on grid I became unreliable at $t \approx 5$). Repeating the same calculation but with $t_s = -\frac{1}{2}\pi$ confirmed the distributions shown in figure 12 to within the resolution of the figure, eliminating the possibility that these waves are a transient phenomenon. Indeed, this correlation between the results for $t_s = 0$ and

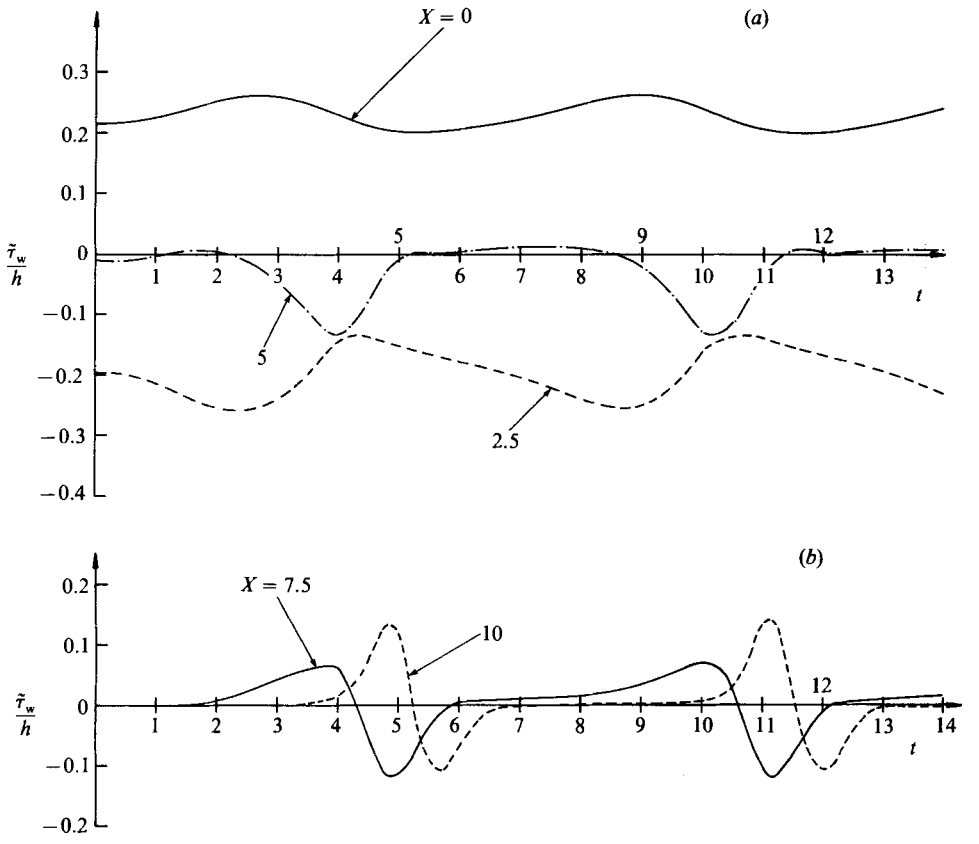

FIGURE 13. (*a*, *b*) Temporal variation of perturbation wall shear; incompressible linear case, $\gamma = 0.5$, $t_s = 0$, $\beta = 1$, profile (4.3), grid I.

$t_s = -\frac{1}{2}\pi$ vindicates the use of the start-up procedure in this case. It is not completely clear why growing Tollmien–Schlichting waves are not excited throughout the entire cycle. A possible explanation is that their growth is enhanced in the presence of an adverse pressure gradient/deceleration of the free-stream flow (see for example Gad-el-Hak *et al.* 1984), and this occurs for $-\pi < t < 0$, $\pi < t < 2\pi$, etc.

The second example of this linearized incompressible type is $\gamma = 0.5$, $\beta = 1$, with profile (4.3). Temporal variations of perturbation wall shear at five selected X-locations are shown in figure 13(*a*, *b*), obtained on grid I with $t_s = 0$. The rapid decay of $F^*(k)$ with k postpones the difficulties associated with the triggering of unstable Tollmien–Schlichting waves since all modes are effectively weighted by a factor e^{-k^2} in spectral space. This particular computation remained reliable until just after $t = 14$, after which large spurious oscillations started to occur in the physical solution. A control computation on grid I remained reliable until just after $t = 10$; however, up to this time the results on this coarser grid agreed to within the graphical accuracy of the results in figure 13. Figure 13(*b*), particularly, suggests that the Tollmien–Schlichting waves are growing in amplitude as they travel downstream, in line with the earlier comments. As with the previous example it does not appear that growing Tollmien–Schlichting waves are being formed continuously, but rather their manufacture is confined to certain periods throughout the cycle. Indeed, these results add some credence to the suggestions above concerning the link between adverse

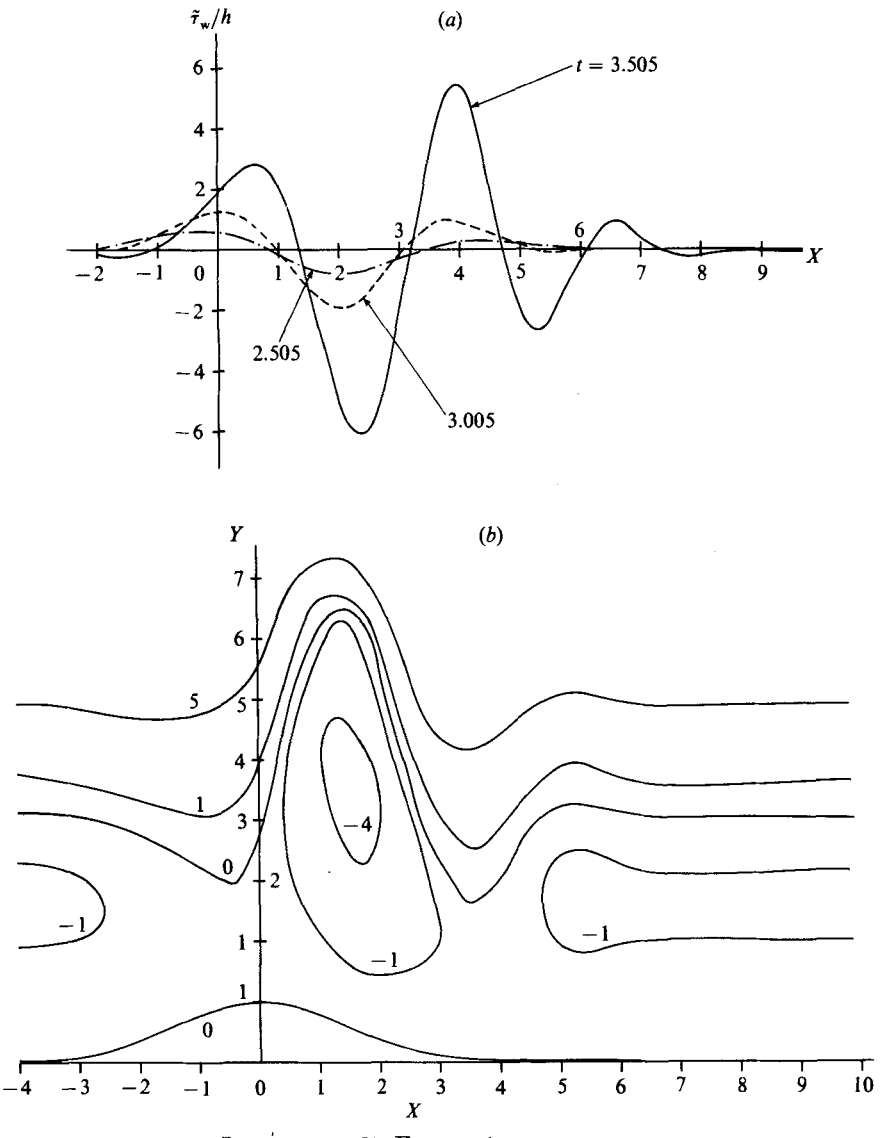

FIGURE 14 (*a*, *b*). For caption see next page.

pressure gradients and the manufacture of Tollmien–Schlichting waves. A further control computation was performed, using grid I and commencing at $t = \frac{1}{2}\pi$ (to check on the effects of transient terms), and this confirmed these conclusions.

The final linearized incompressible example considered here is for the above case, with a larger amplitude parameter, namely $\gamma = 2.5$ ($\beta = 1$, still). Figure 14 (*a*) shows perturbation wall shear distributions, obtained on grid I, with a starting time $t_s = 0$. These show Tollmien–Schlichting waves forming rapidly and growing with travel downstream. Eventually the solution began to exhibit (spurious) upstream oscillations, mirrored in spectral space by the extremely large-amplitude oscillations of the transformed solution. The computation was repeated with $t_s = -\frac{1}{2}\pi$ and the results shown in figure 14 (*a*) were confirmed (to within the resolution of the figure), indicating that the distributions were independent of the start-up process employed,

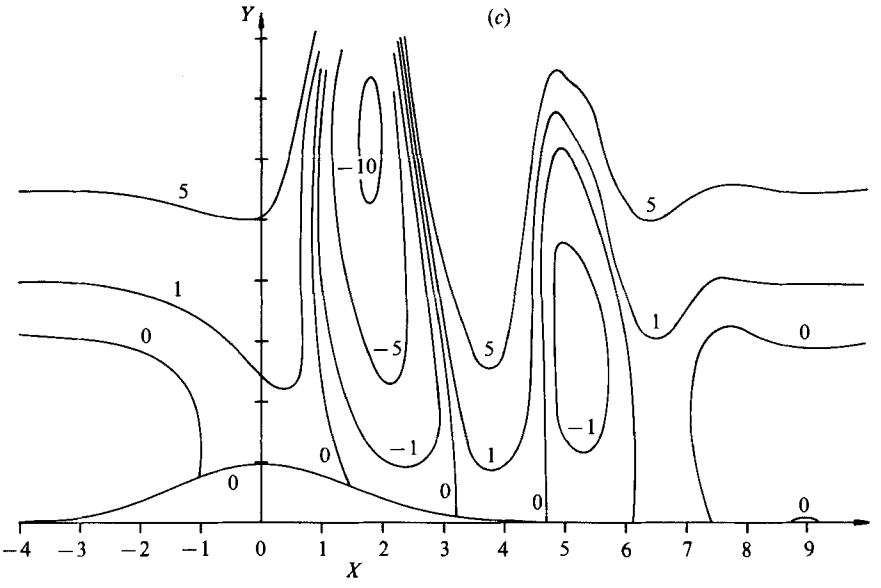

FIGURE 14. (*a*) Distribution of perturbation wall shear; (*b*, *c*) instantaneous streamline pattern at $t = 3.005$, 3.505 respectively. Incompressible linear case, $\gamma = 2.5$, $t_s = 0$, $\beta = 1$, profile (4.3), grid I.

although all computations had to be abandoned (owing to the difficulties with spurious oscillations) before one cycle had been completed.

The streamline patterns corresponding to this example (with a notional height parameter $h = 1$) are shown in figures 14(*b*) and 14(*c*), at $t = 3.005$ and 3.505 respectively. The flow is seen to become increasingly complex, and intensifying away from the surface as the Tollmien–Schlichting waves grow in magnitude and develop. The position of the closed eddies is seen to be approximately in phase with the Tollmien–Schlichting waveform.

These results clearly reveal an increase in the growth rate of the Tollmien–Schlichting instability as the amplitude of the oscillatory flow increases; this is accompanied by increasing difficulty in obtaining accurate numerical solutions at large times after the initiation of the computation.

4.4. *Nonlinear incompressible results*

Just one example of this class is presented, namely the nonlinear version of the second case considered in §4.3, (profile (4.3) with $h = \beta = 1$, $\gamma = 0.5$ and $t_s = 0$). This profile was chosen in preference to (4.1) because of its more favourable computational characteristics as outlined above. This example also provides a direct means of judging the effects of nonlinearity. Results for perturbation wall shear variations with t are shown in figure 15(*a*, *b*) (obtained using grid I), and may be compared directly with figure 13(*a*, *b*). Up to $X = 5$, the nonlinearity has little effect. However further downstream (see figure 15*b* and compare with figure 13*b*), nonlinearity is tending to increase the magnitude of the waves, this effect apparently becoming more pronounced further downstream. As such, nonlinearity can be considered to play a destabilizing role, in line with the general conclusions concerning the effects of nonlinearity on the incompressible cases considered in I.

This particular calculation was abandoned shortly after $t = 6.5$ because of doubts about the accuracy. At this stage, in addition to the increasingly large and rapid

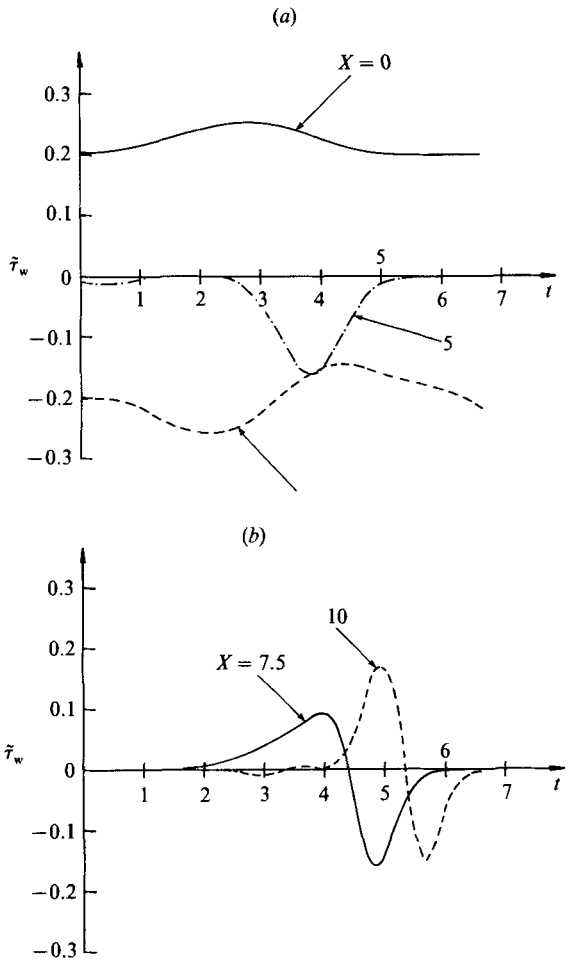

FIGURE 15. (*a*, *b*) Temporal variation of perturbation wall shear, incompressible nonlinear case $\gamma = 0.5$, $t_s = 0$, $h = 1$, $\beta = 1$, profile (4.3), grid I.

oscillations in the spectral solution at finite k (corresponding to the Tollmien–Schlichting instability, which were also encountered in the corresponding linearized results), the $|k| \gg 1$ spectral solution had ceased to decay adequately. This difficulty was not found in the analogous linearized computation and is thus a feature of the nonlinearity. The most likely cause of this effect (and here the study of Duck 1986 serves as a guide) is the Tollmien–Schlichting waves, in particular whose caused by the start-up process, themselves being subject to a secondary instability some distance downstream.

5. General discussion and further comments

It appears that these results illustrate two forms of instability, namely Raleigh and Tollmien–Schlichting type, the latter only being present in incompressible flows of this class.

It is now well known (Smith 1979*a*, *b*) that the lower branch of the neutral stability curve for the Blasius boundary layer in the limit of infinite Reynolds number can be

described by triple-deck theory, and there is increasing evidence that the triple-deck model can provide the basis for investigating further stages of certain transition processes (Smith & Burggraf 1985; Smith 1986; Smith & Stewart 1987; Stewart & Smith 1987). Indeed, the nonlinear incompressible results presented in §4.4 (together with I and Duck 1986) indicate a rapid growth of the spectral solution for large wavenumbers, suggesting the development of a second stage – possibly involving the Tollmien–Schlichting waves being subject to a Rayleigh-type instability. Further, there is increasing evidence that all the four main types of instability – Tollmien–Schlichting waves, Kelvin–Helmholtz waves, Görtler vortices and Rayleigh waves – are inter-related and may evolve from one class to another (Smith 1985).

In the case of the supersonic results, the Tollmien–Schlichting mode of instability is probably not present in the results shown here. The nature of the mechanisms that cause the 'spiking' effect observed in some cases, and the apparent breakdown in others, seems to be associated with a large-wavenumber instability, as borne out by the testing for Rayleigh instabilities. Certain of the examples illustrate the possibility of a small perturbation exciting a rapidly growing Rayleigh instability, although it is not possible to be completely categorical on this point, since Rayleigh modes of instability may be present, and yet breakdown need not necessarily occur. Related to this it seems difficult to predict *a priori* whether a computation will develop an apparent singularity. This may be related to difficulties found in the study (both theoretical and experimental) of the instability of Stokes layers, which have received a good deal of attention in the past.

Von Kerczek & Davis (1974) studied the flow above an oscillatory plate (with an imposed stationary boundary above), and using Floquet theory could find no unstable disturbances. Hall (1978) relaxed the requirement of the upper boundary, but again could find only stable flows. Oscillatory flow through circular pipes has also been studied – by Yang & Yih (1977) (only decaying disturbances found) and Pelissier (1979) (growing disturbances found, but results are of uncertain accuracy).

These (and other) theoretical results do not appear to be in agreement with experimental evidence involving turbulent bursts; for example Li (1954) (channel with oscillatory base); Sergeev (1966), Hino, Sawamoto & Takasu (1976), Iguchi, Ohmi & Megawa (1980), Ohmi *et al.* (1982), Merkli & Thomann (1975), Clarion & Pelissier (1975), (oscillatory flows through pipes). For pulsatile flows, which involve Stokes layers close to the boundaries (a situation similar to the present study), Nerem, Seed & Wood (1972) have recorded turbulent bursts in the canine aorta.

It has been suggested that in Stokes layers where disturbances are subject to a net decay over a full cycle, disturbances can grow significantly over part, if not all of the cycle. This type of argument has been used as a basis for a number of studies by, for example, Rosenblat (1968), Rosenblat & Herbert (1970), Davis & Rosenblat (1972), Hall (1983) and Cowley (1987). This appears to the situation in the present study, where it has been demonstrated that $|k| \gg 1$ instabilities can exist over part of the cycle. At the same time, there is some qualitative correlation between these results and those relating to the stability of shear layers (Betchov 1960; Greenspan & Benney 1963). Indeed, inflexion points were shown to be important in these studies, just as in the case of Rayleigh instability (the profile in the present study has an infinite number of inflexion points at all times).

In the present study, nonlinearity seems generally to enhance the growth of $|k| \gg 1$ modes, and of the associated singularity. Further progress in describing this important process requires a thorough understanding of the positive identification of the singularity (a possible candidate for the structure could be an extension of that

proposed by Brotherton-Ratcliffe & Smith 1987). This is likely to be a difficult task, owing to the requirements for more extensive (and finer) numerical grids as the critical time is approached. However, the spectral method, as used here, has significant advantages in problems of this type over more conventional (i.e. fully finite-difference) methods, and work is underway using this technique to study more fully this aspect of the solution. The occurrence of a singularity of the solution here could lead to some important consequences for the flow, involving possibly a sudden burst of vorticity into the bulk of the fluid. Further, three-dimensional effects will undoubtedly become important, and must ultimately be incorporated into any studies of this process.

This work was partially supported by NATO Grant 523/82. The author wishes to express his gratitude to the referees, and Dr S. J. Cowley, for their comments on a previous version of this paper. A number of the computations were performed under computer time provided by SERC. Grant no. GR/E/25702.

REFERENCES

ACKERBERG, R. C. & PHILLIPS, J. H. 1972 The unsteady boundary layer on a semi-infinite flat plate due to small fluctuations in the magnitude of a free-stream velocity. *J. Fluid Mech.* **51**, 137.

BETCHOV, R. 1960 On the mechanisms of turbulent transition, *Phys. Fluids* **3**, 1026.

BOGDANOVA, E. V. & RYZHOV, O. S. 1983 Free and induced oscillations in Poiseuille flow. *Q. J. Mech. Appl. Maths* **36**, 271.

BROTHERTON-RATCLIFFE, R. V. & SMITH, F. T. 1987 Complete breakdown of an unsteady interactive boundary layer (over a surface distortion or in liquid layer). *Mathematika* **34**, 86.

BROWN, S. N. & CHENG, H. K. 1981 Correlated and steady laminar trailing edge flows. *J. Fluid Mech.* **108**, 171.

BROWN, S. N. & DANIELS, P. G. 1975 On the viscous flow about the trailing edge of a rapidly oscillating plate. *J. Fluid Mech.* **67**, 743.

BROWN, S. N. & STEWARTSON, K. 1973*a* On the propagation of disturbances in a laminar boundary layer I. *Proc. Camb. Phil. Soc.* **73**, 493.

BROWN, S. N. & STEWARTSON, K. 1973*b* On the propagation of disturbances in a laminar boundary layer II. *Proc. Camb. Phil. Soc.* **73**, 505.

BURGGRAF, O. R. & DUCK, P. W. 1981 Spectral computation of triple-deck flows. In *Numerical and Physical Aspects of Aerodynamic flows* (ed. T. Cebeci). Springer.

CLARION, C. & PELISSIER, R. 1975 A theoretical and experimental study of the velocity distribution and transition to turbulence in free oscillatory flow. *J. Fluid Mech.* **70**, 59.

COOLEY, J. W. & TUKEY, J. W. 1965 An algorithm for the machine computation of complex Fourier series. *Math. Comp.* **19**, 297.

COWLEY, S. J. 1981 High Reynolds number flows through channels and flexible tubes. Ph.D. dissertation, University of Cambridge.

COWLEY, S. J. 1985 Pulsatile flow through distorted channels; low-Strouhal-number and translating-critical-layer effects. *Q. J. Mech. Appl. Maths* **38**, 589.

COWLEY, S. J. 1987 High frequency Rayleigh instability of Stokes layers. In *Proc. ICASE Workshop on the Stability of Time Dependent and Spatially Varying Flows.* Springer.

DAVIS, S. H. & ROSENBLAT, S. 1972 On bifurcating periodic solutions at low frequency. *Stud. Appl. Maths* **57**, 59.

DUCK, P. W. 1978 Laminar flow over a small unsteady hump on a flat plate. *Mathematika* **25**, 24.

DUCK, P. W. 1980 Pulsatile flow in constricted or dilated channels. *Q. J. Mech. Appl. Maths* **33**, 78.

DUCK, P. W. 1981 Laminar flow over a small unsteady three-dimensional hump. *Z. angew. Math. Phys.* **32**, 62.

DUCK, P. W. 1985*a* Laminar flow over unsteady humps: the formation of waves. *J. Fluid Mech.* **160**, 465.

DUCK, P. W. 1985*b* Pulsatile flow through constricted or dilated channels: Part II. *Q. J. Mech. Appl. Maths* **38**, 621.

Duck, P. W. 1986 Unsteady triple deck flows leading to instabilities. In *Proc. IUTAM Symp. on Boundary Layer Separation* (ed. S. N. Brown & F. T. Smith). Springer.

GAD-EL-HAK, M., DAVIS, S. H., MCMURRAY, J. T. & ORSZAG, S. A. 1984 On the stability of the decelerating laminar boundary layer. *J. Fluid Mech.* **138**, 297.

GIBSON, W. E. 1957 Unsteady boundary layers. Ph.D. dissertation, M.I.T.

GOLDSTEIN, M. E. 1983 The evolution of Tollmien–Schlichting waves near a leading edge. *J. Fluid Mech.* **127**, 59.

GOLDSTEIN, M. E. 1985 Scattering of acoustic waves into Tollmien–Schlichting waves by small streamwise variations in surface geometry. *J. Fluid Mech.* **154**, 309.

GOLDSTEIN, M. E., POCKOL, P. M. & SANZ, J. 1983 The evolution of Tollmien–Schlichting waves near a leading edge. Part 2. Numerical determination of amplitudes. *J. Fluid Mech.* **129**, 443.

GREENSPAN, H. P. & BENNEY, D. J. 1963 On shear-layer instability, breakdown and transition. *J. Fluid Mech.* **15**, 133.

HALL, P. 1978 The linear stability of flat Stokes layers. *Proc. R. Soc. Lond.* A **359**, 151.

HALL, P. 1983 On the nonlinear stability of slowly varying time-dependent viscous flows. *J. Fluid Mech.* **126**, 357.

HINO, M., SAWAMOTO, M. & TAKASU, S. 1976 Experiments on transition to turbulence in an oscillatory pipe flow. *J. Fluid Mech.* **75**, 193.

IGUCHI, M., OHMI, M. & MEGAWA, K. 1982 Analysis of free oscillating flow in a U shaped tube. *Bull. JSME* **25**, 1398.

ILLINGWORTH, C. R. 1958 The effects of a sound wave on the compressible boundary layer on a flat plate. *J. Fluid Mech.* **3**, 471.

LAM, S. H. & ROTT, N. 1960 Theory of linearized time-dependent boundary layers. *Cornell Univ. GSAE Rep.* AF0512, TN-60-1100.

LI, H. 1954 Stability of oscillatory laminar flow along a wall. *Beach Erosion Board, OS. Army Corps Eng., Washington, D.C. Tech. Memo* 47.

LIGHTHILL, M. J. 1954 The response of laminar skin friction and heat transfer to fluctuations in the stream velocity. *Proc. R. Soc. Lond.* A **224**, 1.

LIN, C. C. 1956 Motion in the boundary layer with a rapidly oscillating external flow. *Proc. IXth Int. Cong. Appl. Mech. Brussels*, vol. 4, p. 155.

MERKLI, P. & THOMANN, H. 1975 Transition to turbulence in oscillating pipe flow. *J. Fluid Mech.* **68**, 567.

MOORE, F. K. 1951 Unsteady laminar boundary layer flow. *NACA Tech. Note* 2471.

MOORE, F. K. 1957 Aerodynamic effects of boundary-layer unsteadiness. *Proc. 6th Anglo. Amer. Conf. Roy. Aero. Soc., Folkestone*, p. 439.

MURDOCH, J. W. 1980 The generation of a Tollmien–Schlichting wave by a sound wave. *Proc. R. Soc. Lond.* A **372**, 517.

NEREM, R., SEED, W. A. & WOOD, N. B. 1972 An experimental study of the velocity distribution and transition to turbulence in the aorta. *J. Fluid Mech.* **52**, 137.

OHMI, M., IGUCHI, M., KAKEHASHI, K. & MASUDA, T. 1982 Transition to turbulence and velocity distribution in an oscillating pipe flow. *Bull. JSME* **25**, 365.

PEDLEY, T. J. 1972 Two-dimensional boundary layers in a free stream which oscillates without reversing. *J. Fluid Mech.* **55**, 359.

PELISSIER, R. 1979 Stability of a pseudo-periodic flow. *Z. angew. Math. Phys.* **30**, 577.

ROSENBLAT, S. 1968 Centrifugal instability of time-dependent flows. Part 1. Inviscid, periodic flows. *J. Fluid Mech.* **33**, 321.

ROSENBLAT, S. & HERBERT, D. M. 1970 Low frequency modulation of thermal instability. *J. Fluid Mech.* **43**, 385.

ROSENHEAD, L. (ed.) 1963 *Laminar Boundary Layers.* Oxford University Press.

RYZHOV, O. S. & ZHUK, V. I. 1980 Internal waves in a boundary layer with the self-induced pressure. *J. Méc.* **19**, 561.

SERGEEV, S. I. 1966 Fluid oscillations in pipes at moderate Reynolds numbers. *Mekh. Zhidk. Gaza* **1**, 168 (Transl. *Fluid Dyn.* **1**, 121).

SOBEY, I. J. 1980 On the flow through furrowed channels. Part 1. Calculated flow patterns. *J. Fluid Mech.* **96**, 1.

SOBEY, I. J. 1982 Oscillatory flows at intermediate Strouhal numbers in asymmetric channels. *J. Fluid Mech.* **125**, 359.

SOBEY, I. J. 1985 Observation of waves during oscillatory channel flow. *J. Fluid. Mech.* **151**, 395.

SMITH, F. T. 1973 Laminar flow over a small hump on a flat plate. *J. Fluid Mech.* **57**, 803.

SMITH, F. T. 1979*a* Nonlinear stability of boundary layers for disturbances of various sizes. *Proc. R. Soc. Lond.* A **368**, 573. (See also *Proc. R. Soc. Lond.* A **371** (1980), 439.)

SMITH, F. T. 1979*b* On the non-parallel flow stability of the Blasius boundary layers. *Proc. R. Soc. Lond.* A **366**, 91.

SMITH, F. T. 1985 Non-linear effects and non-parallel flows: the collapse of separating motion. *United Technologies Research Centre Rep.*

SMITH, F. T. 1986 Two-dimensional disturbance travel, growth and spreading of boundary layers. *J. Fluid Mech.* **169**, 353.

SMITH, F. T. & BODONYI, R. J. 1985 On short scale inviscid instabilities in flow past surface-mounted obstacles and other non-parallel motions. *Aero. Q.* **36**, 205.

SMITH, F. T. & BURGGRAF, O. R. 1985 On the development of large-sized short-scaled disturbances in boundary layers. *Proc. R. Soc. Lond.* A **399**, 25.

SMITH, F. T. & STEWART, P. A. 1987 The resonant-triad nonlinear interaction in boundary-layer transition. *J. Fluid Mech.* **179**, 227.

STEWART, P. A. & SMITH, F. T. 1987 Three-dimensional instabilities in steady and unsteady non-parallel boundary layers including effects of Tollmien–Schlichting disturbances and cross flow. *Proc. R. Soc. Lond.* A **409**, 299.

STEWARTSON, K. 1969 On the flow near the trailing edge of a flat plate – II. *Mathematika* **16**, 106.

STEWARTSON, K. & WILLIAMS, P. G. 1969 Self-induced separation. *Proc. R. Soc. Lond.* A **312**, 181.

TERENT'EV, E. D. 1978 On an unsteady boundary layer with self-induced pressure in the vicinity of a vibrating wall in a supersonic flow (in Russian). *Dokl. Akad. Nauk. SSSR* **240**, 1046.

TERENT'EV, E. D. 1984 Linear problem on vibrator on a flat plate in subsonic boundary layer. In *Proc. IUTAM Symp. Laminar–Turbulent Transition Novosibrisk 1984* (ed. V. V. Kozlov). Springer.

TUTTY, O. R. & COWLEY, S. J. 1986 On the stability and numerical solution of the unsteady interactive boundary-layer equation. *J. Fluid Mech.* **168**, 431.

VON KERCZEK, C. & DAVIS, S. H. 1974 Linear stability theory of oscillatory Stokes layers. *J. Fluid Mech.* **62**, 753.

YANG, W. H. & YIH, C.-S. 1977 Stability of time-periodic flows in a circular pipe. *J. Fluid Mech.* **82**, 497.

ZHUK, V. I. & RYZHOV, O. S. 1978 On one property of the linearised boundary-layer equations with a self-induced pressure (in Russian). *Dokl. Akad. Nauk SSSR* **240**, 1042.